

A resolution of puzzles from the LSND, KARMEN, and MiniBooNE experiments

S.N. Gninenko

Institute for Nuclear Research, Moscow 117312

(Dated: October 10, 2018)

This work has attempted to reconcile puzzling neutrino oscillation results from the LSND, KARMEN and MiniBooNE experiments. We show that the LSND evidence for $\bar{\nu}_\mu \rightarrow \bar{\nu}_e$ oscillations, its long-standing disagreement with the results from KARMEN, and the anomalous event excess observed by MiniBooNE in ν_μ and $\bar{\nu}_\mu$ data, all could be explained by the existence of a heavy sterile neutrino (ν_h). These results are found to be consistent with each other assuming that the ν_h is created by mixing in ν_μ neutral-current interactions and decays radiatively into a photon and a light neutrino. Combined analysis of the LSND and MiniBooNE excess events suggests that the ν_h mass is in the range from 40 to 80 MeV, the mixing strength is $|U_{\mu h}|^2 \simeq 10^{-3} - 10^{-2}$ and the lifetime $\tau_{\nu_h} \lesssim 10^{-9}$ s. Surprisingly, this LSND-MiniBooNE parameters window is found to be unconstrained by the results from the most sensitive experiments searching for heavy neutrino. We set new limits on $|U_{\mu h}|^2$ for the LSND-MiniBooNE favorable mass region from the precision measurements of the Michel spectrum by the TWIST experiment. The results obtained provide strong motivation for a sensitive search for the ν_h in a near future K decay or neutrino experiments, which fit well in the existing/planned experimental programs at CERN or FNAL. The question of whether the heavy neutrino is Dirac or Majorana particle is briefly discussed.

PACS numbers: 14.80.-j, 12.60.-i, 13.20.Cz, 13.35.Hb

I. INTRODUCTION

Over the past 10 years there is a puzzle of the 3.8 σ event excess observed by the LSND collaboration [1] at LANSCE [2, 3]. This excess originally interpreted as a signal from $\bar{\nu}_\mu \rightarrow \bar{\nu}_e$ oscillations was not confirmed by further measurements from the similar experiment KARMEN [4], which was running at the ISIS neutron spallation facility of the RAL [5]. The MiniBooNE experiment at FNAL [6], designed to examine the LSND effect, did not find evidence for $\nu_\mu \rightarrow \nu_e$ oscillations. However, an anomalous excess of low energy electron-like events in charge-current quasi-elastic ($CCQE$) neutrino events over the expected standard neutrino interactions has been observed [7]. This MiniBooNE anomaly has been confirmed by the finding of more excess events [8]. While the collaboration has not yet clarified the origin of the excess, several models involving new physics were considered to explain the discrepancy, see [8] and references therein. Recently, the MiniBooNE experiment has reported new results from a search for $\bar{\nu}_\mu \rightarrow \bar{\nu}_e$ oscillations [9]. An excess of events is observed, which has a small probability for consistency with the background-only hypothesis. The data are found to be consistent with $\bar{\nu}_\mu \rightarrow \bar{\nu}_e$ oscillations in the 0.1 eV range and with the evidence for antineutrino oscillations from the LSND.

The new observations bring more confusion than clarity to the experimental situation. Inconsistency between the results, in particular from the LSND and KARMEN, is also confusing in light of the apparent simplicity of the primary reaction, $p(\bar{\nu}_e, e)n$, used by these experiments for the oscillation signal search, and also in view of the fact that other results, e.g. inclusive cross section

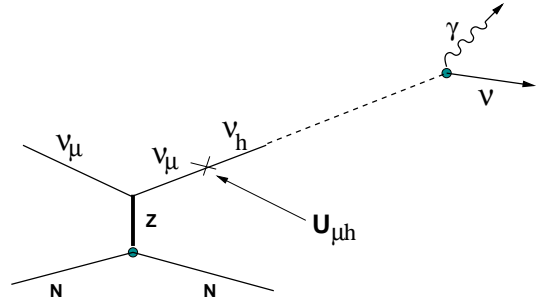


FIG. 1: Schematic illustration of the $NCQE$ production and decay of heavy neutrino.

for the reactions $^{12}C(\nu_e, e)^{12}N^*$ with electrons in the final state, measured by LSND [10] and KARMEN [11], agree quite well with each other and also with theoretical calculations. To reconcile LSND, KARMEN and MiniBooNE results in terms of the, so-called (3+1)- ν oscillations scheme or (yet unknown) experimental background seems is quite difficult [12]. Therefore, any new explanation involving new physics deserves to be considered seriously.

This work has attempted to reconcile puzzling neutrino oscillation results from the LSND, KARMEN and MiniBooNE experiments. As an input, we use a natural extension of the model developed in Ref.[13] for explanation of the MiniBooNE anomaly observed in ν_μ data in terms of radiative decays of $\simeq 500$ MeV sterile neutrino (ν_h). Our discussion is based on the fact that in these experiments the signals produced by electrons or by converted photons are indistinguishable. This hint suggests that the excess events could originate from con-

verted photons, and not from electrons. Being motivated by the above considerations, we show that the LSND evidence for $\bar{\nu}_\mu \rightarrow \bar{\nu}_e$ oscillations, its long-standing disagreement with the results from KARMEN, and the anomalous event excess observed by MiniBooNE in ν_μ and $\bar{\nu}_\mu$ data, all could be explained by the existence of a heavy sterile neutrino (ν_h). All these observations are found to be consistent with each other assuming that ν_h 's are produced by muonic mixing in ν_μ neutral-current interactions and decay radiatively into a photon and a light neutrino ν , as shown in Fig.1.

It is known, that the neutrino weak flavor eigenstates ($\nu_e, \nu_\mu, \nu_\tau, \dots$) can be different from the mass eigenstates ($\nu_1, \nu_2, \nu_3, \nu_4, \dots$), but they are related to them, in general, through a unitary transformation. A generalized mixing:

$$\nu_l = \sum_i U_{li} \nu_i; \quad l = e, \mu, \tau, \dots, \quad i = 1, 2, 3, 4, \dots \quad (1)$$

results in neutrino oscillations when the mass differences are small, and in neutrino decays when the mass differences are large. If the ν_h is a component of ν_μ , it would be produced by any source of ν_μ according to the proper mixing $|U_{\mu h}|^2$ and a phase space factor, as follows from Eq. (1). In particular, ν_h could be produced in neutrino neutral current (NC) interactions or any leptonic and semileptonic decays of sufficiently heavy mesons and baryons [14], see also [15]. The ν_h 's could be Dirac or Majorana type and decay dominantly into $\nu_h \rightarrow \gamma \nu$ in the detector target if, for example, there is a non-zero transition magnetic moment (μ_{tr}) between the ν_h and an active neutrino ν [16, 17]. Such type of neutrinos are present in many interesting extensions of the Standard Model, such as GUT, Superstring inspired models, Left-Right Symmetric models and others, see e.g. Ref.[16].

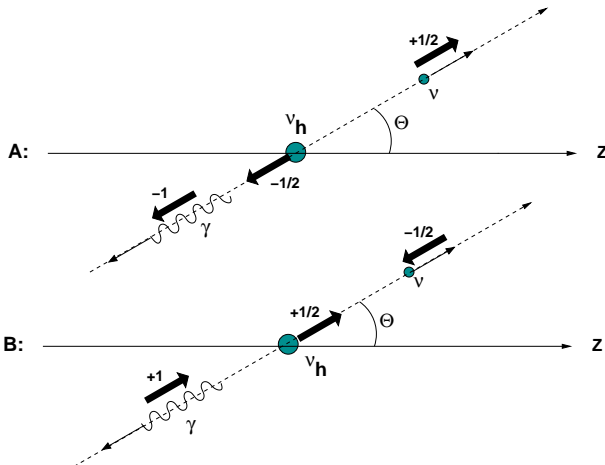


FIG. 2: Two amplitudes A and B describing the decay $\nu_h \rightarrow \gamma \nu$ for different ν_h helicities.

The rest of the paper is organized as follows. In Sec.II we describe the formalism for the radiative neutrino de-

cay, specifying the difference between the Dirac and Majorana decay modes. The results from the LSND and KARMEN experiments are described in Sec.III. Here we show how the model suggested explain those results. In Sec.IV we briefly describe the MiniBooNE experiment and give an explanation of the anomalous excess of events observed in ν_μ and $\bar{\nu}_\mu$ data. The final results from the combined analysis of the LSND and MiniBooNE data are reported in Sec.V. The discussion and review of the experimental constraints on the mixing strength $|U_{\mu h}|^2$ are presented in Sec.VI. We find that, quite surprisingly, the $(m_{\nu_h}; |U_{\mu h}|^2)$ parameter space favorable for explanation of the LSND and MiniBooNE results is unconstrained by the results from the most sensitive experiments, e.g. searching for a ν_h peak in $\pi_{\mu 2}, K_{\mu 2}$ decays. Moreover, we show that taking into account the dominance of $\nu_h \rightarrow \gamma \nu$ decay and the short ν_h lifetime make existing experimental bounds weaker allowing to extend them to the higher mass region. In Sec.VII, several proposed experiments to search for the ν_h and the decay $\nu_h \rightarrow \gamma \nu$ are described. We also show that, several tests can be applied to existing data. A model for the radiative ν_h decay is discussed in Sec. VIII. Sec.IX contains concluding remarks.

II. RADIATIVE NEUTRINO DECAY AND FORWARD-BACKWARD PHOTON ASYMMETRY

Let us consider the decay of a heavy neutrino, ν_h of mass m_{ν_h} and energy E into a lighter neutrino ν and a photon:

$$\nu_h \rightarrow \nu + \gamma \quad (2)$$

with the partial lifetime τ_{ν_h} .

The energy of the decay photon in the ν_h rest frame is $0 \leq E_\gamma \leq m_{\nu_h}/2$, depending on the mass of the ν . Furthermore, we assume the particle ν is almost massless, and the photon energy is $E_\gamma = m_{\nu_h}/2$.

The decay of a spin- $\frac{1}{2}$ neutrino into another spin- $\frac{1}{2}$ particle and a photon can be generally described by two helicity amplitudes A and B corresponding to the final states shown in Fig. 2. For the most general coupling given by [19]-[21]

$$\bar{\psi}(\nu) \sigma_{\mu\nu} (\alpha + \beta \gamma_5) \psi(\nu_h) \partial^\mu A^\nu \quad (3)$$

the amplitudes A and B are proportional, respectively to $(\alpha - \beta)$ and $(\alpha + \beta)$. In the standard model $\beta/\alpha = (m_{\nu_h} - m_\nu)/(m_{\nu_h} + m_\nu)$ [20], so that

$$a^{SM} = \frac{m_{\nu_h}^2 - m_\nu^2}{m_{\nu_h}^2 + m_\nu^2} \quad (4)$$

The energy distribution of photons in the laboratory system depends on their angular distribution in the rest frame, which is not generally isotropic [18]:

$$\frac{dN}{d\cos\Theta} = \frac{1}{2}(1 + a\cos\Theta) \quad (5)$$

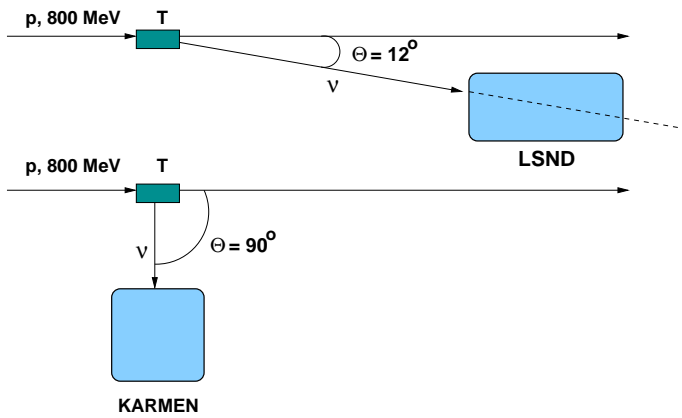


FIG. 3: Schematic illustration of the location of the LSND and KARMEN detectors relative to the primary proton beam direction.

where Θ is the angle in the center-of-mass system between the photon momentum and the beam direction and a is the asymmetry parameter.

Assuming CPT conservation implies $|A| = |B|$ for Majorana neutrinos. In this case the decay would be isotropic and independent of the ν_h polarization, and hence $a = 0$ in Eq.(5). However, for Dirac neutrinos the asymmetry parameter

$$a = -2 \frac{\text{Re}(\alpha^* \beta)}{|\alpha|^2 + |\beta|^2} \quad (6)$$

is not constrained, and it may be in the range $-1 < a < +1$ [19, 20]. The angular anisotropy is the result of parity non-conservation in the decay (2) and of non-vanishing polarization of the neutrinos.

For left-handed Dirac neutrinos and massless ν , one has $a = -1$, which means that the decay photons are emitted preferably backward [19]-[21], and the energy spectrum in the laboratory frame becomes softer. For the right-handed Dirac neutrinos one has $a = +1$, and the photons are emitted preferably in the forward direction and the laboratory frame spectrum becomes harder. Hence, the energy spectrum of decay photons is sensitive to the type of the ν_h .

Note, that if CP is conserved, the decay rate and the center-of-mass angular distributions for Dirac case are the same for $\nu_h \rightarrow \gamma \nu$ as for $\bar{\nu}_h \rightarrow \bar{\nu} \gamma$ decay modes. Furthermore, we assume that the ν_h produced in the NC interactions preserves the helicity of the incoming neutrino, and the decay $\nu_h \rightarrow \gamma \nu$ is generally CP -conserving (see, also Sec.IV.B).

III. INTERPRETATION OF THE LSND AND KARMEN RESULTS

The LSND [22] and KARMEN [5] experiments used neutrinos produced in the beam stop of a proton accelerator. LSND has finished data taking at LANSCE at the

end of 1998, while KARMEN has finished data taking in the year 2001. In these experiments, neutrinos were produced by the following decays of pions and muons occurred in the proton target:

- $\pi^+ \rightarrow \mu^+ \nu_\mu$ decays in flight (DIF) or at rest (DAR)
- $\mu^+ \rightarrow e^+ \nu_e \bar{\nu}_\mu$ DAR
- $\pi^- \rightarrow \mu^- \bar{\nu}_\mu$ DIF
- $\mu^- \rightarrow e^- \bar{\nu}_e \nu_\mu$ DAR

The main detector properties and the neutrino fluxes in these experiments are summarized in Table 1.

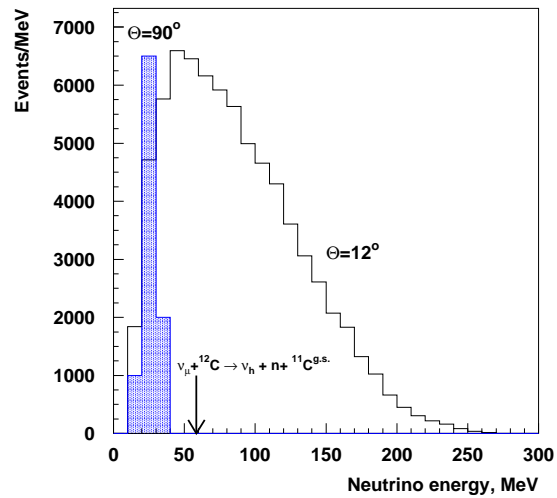


FIG. 4: The energy distributions of ν_μ 's from π^+ DIF in the LSND ($\Theta = 12^\circ$) and KARMEN ($\Theta = 90^\circ$, hatched) detectors. The arrow shows the production threshold of $E_{th} = 58.6$ MeV for the heavy neutrino with the mass of 40 MeV in the reaction $\nu_\mu + {}^{12}\text{C} \rightarrow \nu_h + n + {}^{11}\text{C}_{g.s.}$, in which the ν_h production is accompanied by the emission of a neutron and the isotope ${}^{11}\text{C}$ in the ground state.

A. The LSND signal of $\bar{\nu}_\mu \rightarrow \bar{\nu}_e$ oscillations

In 1996 the LSND experiment published an evidence for $\bar{\nu}_\mu \rightarrow \bar{\nu}_e$ oscillations, based on the observation of an excess of $\bar{\nu}_e$ -like events [2]. Measurements performed in 1996-98 with a different target configuration confirmed the evidence and improved the significance of the observed excess.

The LSND detector is described in details in Ref. [22]. It was located at a distance of 30 m downstream of the main LANSCE beam - stop A6 at a small angle of $\simeq 12^\circ$ relative to the primary proton beam. The detector was a cylindrical volume filled with 167 t of a dilute mineral oil (CH_2) based liquid scintillator viewed by photomultipliers and surrounded by an active 4π veto shield. The low

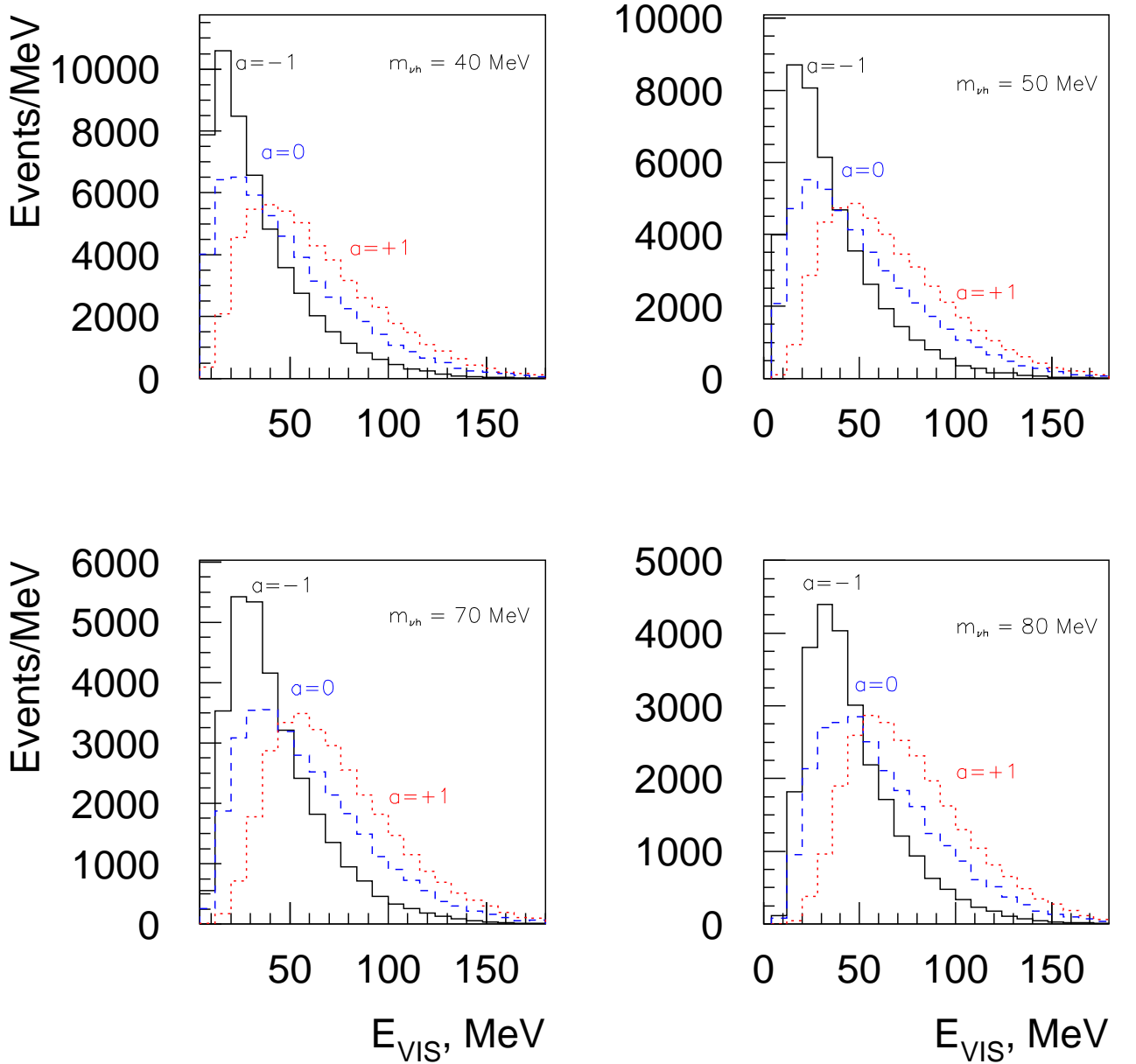


FIG. 5: Distributions of the visible energy in the LSND detector from the $\nu_h \rightarrow \gamma \nu$ decay of sterile neutrino produced in the reaction (7) for different ν_h masses shown in the plots. The spectra are calculated for Dirac ($a = -1$, solid and $a = 1$, dotted) and Majorana ($a = 0$, dashed) cases.

light-yield of the the scintillator allowed to the detection of Cherenkov light generated by relativistic muons, electrons and by converted photon tracks. This feature was of great importance for particle identification and reconstruction of its direction. The energy resolution of the detector was about $\simeq 6\%$ at 50 MeV electron energy.

The search for $\bar{\nu}_\mu \rightarrow \bar{\nu}_e$ oscillations was based on $\bar{\nu}_e$ appearance in the neutrino beam, detected through the reaction $\bar{\nu}_e p \rightarrow e^+ n$ resulting in a prompt relativistic e^+ ,

followed by a 2.2 MeV gamma signal from the neutron capture $p(n, \gamma)d$. The e^+ candidate events identification and separation from the background was based on the detection of the prompt and directional Cherenkov light, and scintillation light which is delayed and isotropic. The 2.2 MeV signal from the reaction $p(n, \gamma)d$ is correlated in time with the positron one. It was identified and separated from accidental low-energy γ 's by means of a likelihood parameter R_γ , which is defined as the ratio of the

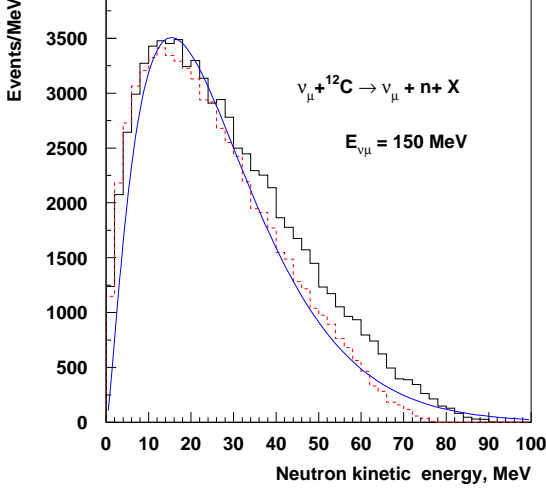


FIG. 6: Distributions of the recoil neutron kinetic energy in the reaction $\nu_\mu^{12}C \rightarrow \nu_\mu nX$ obtained in the present work (solid histogram) and calculated in [26] (solid curve) for the ν_μ energy $E_\nu=150$ MeV. The distribution of the kinetic energy of neutrons ejected in the reaction $\nu_\mu^{12}C \rightarrow \nu_h nX$ for the heavy neutrino mass of 60 MeV is also shown for comparison (dashed histogram). The binding energy corrections are not applied.

likelihood of a low-energy event being correlated or being accidental. The parameter R_γ was defined by three values i) the PMT multiplicity, which is proportional to the γ -energy, ii) the radial distance between the reconstructed positions of the e^+ and γ , and iii) the time difference between the e^+ and γ , which is defined by the capture time of 186 μ s of neutrons in mineral oil, while accidentals are distributed uniformly in time.

A χ^2 fit to the R_γ distribution obtained from the 1993-98 measurements resulted, after subtraction of background from DAR and DIF neutrino events, (19.5 ± 3.9) and (10.5 ± 4.6) , respectively, in a beam on-off excess of $(87.9 \pm 22.4 \pm 6.0)$ events. The neutrino background was carefully evaluated in part from independent measurements and in part from calculations. This excess was attributed to be $\bar{\nu}_e$ appearance from $\bar{\nu}_\mu \rightarrow \bar{\nu}_e$ oscillations and corresponds to the oscillation probability $P(\bar{\nu}_\mu \rightarrow \bar{\nu}_e) = (2.64 \pm 0.67 \pm 0.45) \times 10^{-3}$.

The KARMEN experiment used the similar technique as the LSND and observed no beam excess [5]. The signatures of the 15 candidate events were found to be in a good agreement with those from the (15.8 ± 0.5) expected background events.

Let us explain the discrepancy between the results of these two experiments in terms of the production and radiative decay of a heavy neutrino, as illustrated in Fig.1. The location of the LSND and KARMEN detectors relative to their proton beam directions is schematically illustrated in Fig. 3. The energy distributions of ν_μ 's from

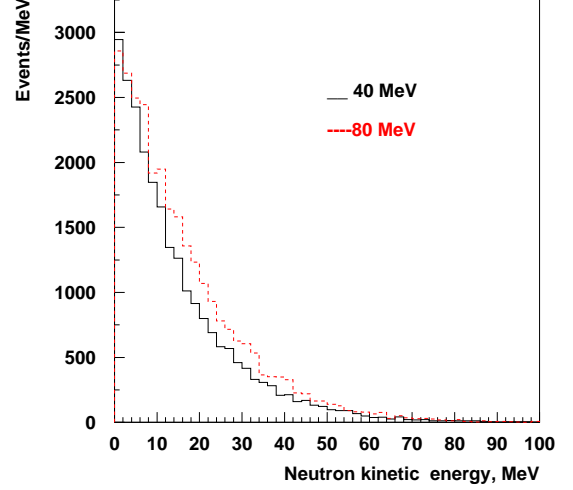


FIG. 7: The ν_μ flux-averaged distributions of the recoil neutron kinetic energy from the reaction $\nu_\mu^{12}C \rightarrow \nu_\mu nX$ calculated for ν_h masses of 40 and 80 MeV with the binding energy correction included.

π^+ DIF in the LSND (from Ref.[23]) and KARMEN (simulated) detectors are shown in Fig.4. One can see that the spectra are quite different. The LSND distribution is peaked at about 55 MeV, it has the average energy $\simeq 100$ MeV, and a high energy tail up to ~ 300 MeV. While the maximum of the energy spectrum in KARMEN, which is located at 90° with respect to the beam, is $\simeq 20$ MeV and the whole spectrum is well below 50 MeV. For the heavy neutrino with the mass $m_{\nu_h} = 40$ MeV, the production threshold in the reaction $\nu_\mu^{12}C \rightarrow \nu_h n^{11}C_{g.s.}$ is 58.6 MeV, as shown in Fig.4. Here we assume, that the ν_h production is accompanied by the emission of a recoil neutron and the isotope ^{11}C in the ground state.

Thus, our interpretation of the excess of events observed by LSND is the following. Positive pions generated in proton collisions produce the flux of ν_μ 's from the $\pi^+ \rightarrow \mu^+ \nu_\mu$ DIF in the target. The excess events are generated in the LSND detector by these ν_μ 's through the reaction

$$\nu_\mu^{12}C \rightarrow \nu_h nX \rightarrow \gamma \nu nX, \quad (7)$$

with the emission of a recoil neutron and the heavy neutrino, and not by $\bar{\nu}_\mu$'s from muon decays at rest via $\bar{\nu}_\mu \rightarrow \bar{\nu}_e$ oscillations, as was originally assumed [3]. The ν_h 's decay promptly into a photon and a light neutrino with the subsequent Compton scattering or e^+e^- pair conversion of the decay photon in the detector fiducial volume. The former process dominates for photon energies below the critical energy of the LSND liquid of 85 MeV. In the laboratory system, the differential Compton scattering cross section has a sharp peak in the forward direction and the vast majority of events are in a narrow cone of $\lesssim \sqrt{m_e/E_\gamma} \lesssim 100$ mrad, for $E_\gamma > 20$ MeV.

TABLE I: Comparison of experimental parameters of the LSND and KARMEN experiments.

	LSND	KARMEN
p beam kinetic energy, MeV	800	800
total number of POT's	1.8×10^{23}	5.9×10^{22}
distance to target, m	30	17
angle between the ν and p beams	12°	90°
total $\bar{\nu}_\mu$ flux	1.2×10^{22}	2.71×10^{21}
$\bar{\nu}_\mu, \nu_e/cm^2$ from μ^+ DAR	1.26×10^{14}	8.86×10^{13}
$\nu_\mu, \bar{\nu}_e/cm^2$ from μ^- DAR	1.08×10^{11}	7.6×10^{10}
ν_μ/cm^2 from π^+ DIF	2.2×10^{12}	$< 10^{11}$
$\bar{\nu}_e p \rightarrow e^+ n$ efficiency	0.17	0.19
e^+ energy range, MeV	20 - 60	16 - 50
beam-on excess	87	15
expected background	53.8	15.8 ± 0.5
event excess	32.2 ± 9.4	$< 5.1(90\% \text{ CL.})$
$\bar{\nu}_\mu \rightarrow \bar{\nu}_e$ oscillation probability	$(0.264 \pm 0.067 \pm 0.045) \times 10^{-3}$	$< 0.85 \times 10^{-3}(90\% \text{ CL.})$

For the photon conversion into a e^+e^- pair its opening angle is $\simeq m_e/E_\gamma < 25$ mrad for $E_\gamma > 20$ MeV, which is too small to be resolved in LSND into two separate Cherenkov rings (here, m_e, E_γ are the electron mass and the photon energy, respectively). Thus, the excess events are originated from photons of the reaction (7), misidentified as single electron events, and detected in coincidence with the associated 2.2 MeV γ tag from the neutron capture. In the KARMEN experiment, ν_μ 's from π decays in flight cannot produce heavy neutrinos accompanied by the emission of a neutron because their energy is less than the ν_h production threshold, see Fig. 4. Therefore, KARMEN should observe no excess of $\bar{\nu}_\mu \rightarrow \bar{\nu}_e$ like events. Note, that the maximum energy of $\bar{\nu}_\mu$'s from muon DAR is about 50 MeV and is also less than the energy threshold of 58.6 MeV for production of the 40 MeV ν_h and a recoil neutron in collisions with the carbon nucleus.

To make quantitative estimates, we performed simplified simulations of the ν_h production in the inclusive reaction (7) with the emission of a recoil neutron and followed by the decay $\nu_h \rightarrow \gamma\nu$, as shown in Fig. 1, in the LSND detector. In these simulations we used the integral ν_μ DIF energy spectrum, shown in Fig. 4, which was calculated in [23]. For the most of the ν_μ 's their energy is well above the production threshold of the 40-80 MeV ν_h 's in the LSND detector. Being produced, the ν_h 's decay at the average distance $L_d \simeq c\tau_h E_{\nu_h}/m_{\nu_h}$ from the primary vertex. Since in the LSND experiment the average ν_h energy is $E_{\nu_h} \simeq 50$ MeV and ν_h 's would decay over the average distance of $\lesssim 5$ m from the primary vertex, the sensitivity is restricted to the ν_h lifetimes $\tau_{\nu_h} \lesssim 10^{-8}$ s for the ν_h masses $m_{\nu_h} \gtrsim 40$ MeV. The decay photon absorption occurs at a distance of the order of the radiation length ($\simeq 40$ cm) of the LSND liquid from the ν_h decay point which is $\ll L_d$.

In Fig. 5 the distributions of the photon energy deposited in the LSND detector calculated for different ν_h masses and decay asymmetry parameters $a = \pm 1$ and $a = 0$ are shown. One can see that for Dirac case with $a = -1$, the simulated excess events are mainly

distributed in the narrow region $0 \lesssim E_{vis} \lesssim 60$ MeV. The fraction of events in this region varies from 0.86 to 0.77 for the ν_h masses from 40 to 80 MeV, respectively. The remaining events are distributed over the region $60 \lesssim E_{vis} \lesssim 150$ MeV, where they can be hidden by the low statistics. For Majorana and Dirac ($a=1$) cases, the fraction of events in the region $0 \lesssim E_{vis} \lesssim 60$ MeV varies from 0.71 to 0.57, and from 0.54 to 0.46, respectively. Further, we will consider only the cases with $a = -1$ and $a = 0$ because for the case $a = +1$ the fraction of events above 60 MeV is too high compare to the LSND observations.

The crucial test of the $\bar{\nu}_\mu \rightarrow \bar{\nu}_e$ oscillation hypothesis in the LSND experiment was to check whether there is an excess of events with more than one correlated 2.2 MeV γ 's. If the excess of events is indeed due to the reaction $\bar{\nu}_e p \rightarrow e^+ n$, then there should be no excess with more than one correlated γ because the recoil neutron is too low in energy (< 5 MeV) to knock out additional neutrons. If, on the other hand, the excess involves higher energy neutrons, which can break the ^{12}C nucleus and produce another neutron(s), then one would expect an excess of events with > 1 correlated γ . As the LSND did not observed many such (latter) events [3], the energy spectrum of ejected neutrons is an important characteristic of the reaction (7), as it affects the likelihood ratio R_γ and the number of correlated γ 's. The ν_μ flux averaged cross sections and particle emission spectra in the LSND detector are predicted quit well for the charge current reactions $\nu_\mu^{12}\text{C} \rightarrow \mu X$ from calculations performed in different theoretical frameworks, see e.g. Ref.[24] and references therein. However, much less is known for the ν_μ induced neutral current reactions in the detector. Therefore, we have performed simulations of the distributions of the kinetic energy of the emitted neutrons in the reaction (7) by using the Fermi gas nuclei model, however without taking into account nuclear effects, such e.g. as the neutron re-scattering in nuclear matter and the carbon nucleus level structure. The Fermi momentum and the neutron binding energy for the ^{12}C nucleus are taken

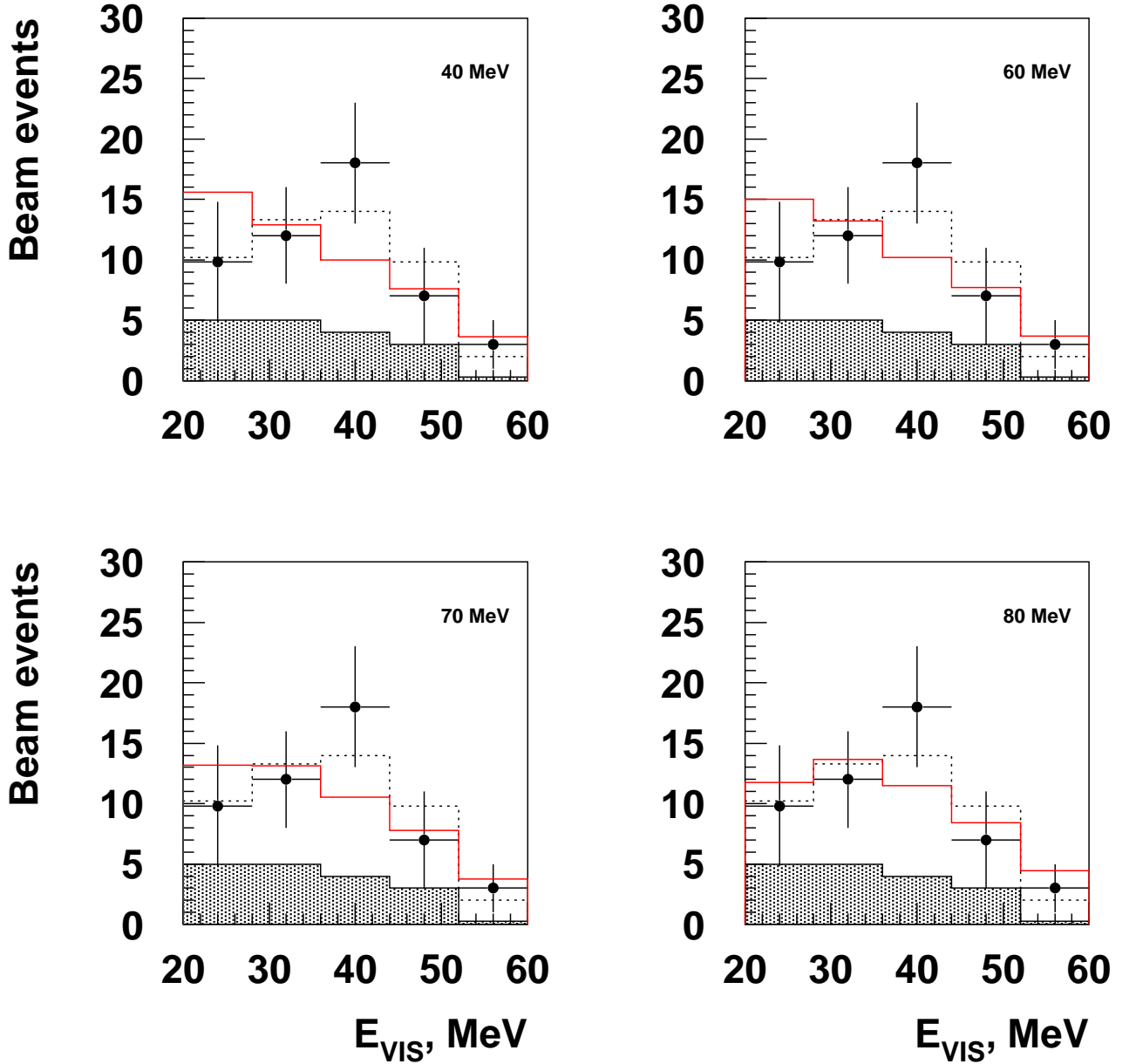


FIG. 8: Distributions of the excess events reconstructed as $\bar{\nu}_e CC$ events in the LSND detector as a function of visible energy E_{vis} for $R_\gamma > 10$ from the 1993-98 data sample (dots), and a combination of $\nu_h \rightarrow \gamma\nu$ decay of DIRAC sterile neutrino ($a = -1$) plus neutrino background (solid) for different ν_h masses shown in the plots, the mixing strength $|U_{\mu h}|^2 = 3 \times 10^{-3}$ and the ν_h lifetime $\tau_{\nu_h} = 10^{-9}$ s. A combination of neutrino background plus neutrino oscillations at low Δm^2 (dashed) and the expected distribution from neutrino background (shaded) from Ref. [3] are also shown.

to be 200 MeV and 18 MeV, respectively.

To evaluate uncertainties of our calculations we have compared our results with others obtained by taking into account nuclear effects [25]-[28]. Fig.6 shows the distribution of the kinetic energy of neutrons ejected in the reaction $\nu_\mu^{12}C \rightarrow \nu_\mu n X$ obtained in the present work and the analogous spectrum from Ref.[26], both calculated for

the massless case for the incident neutrino energy of 150 MeV without nucleon binding energy corrections. One can see that our simulations reproduce the more precise results quite reasonably. The comparison of the calculations results in an uncertainty of about 20-30%. Fig.6 also shows the neutron energy distribution calculated for the reaction (7) for the ν_h mass of 60 MeV. It is seen that

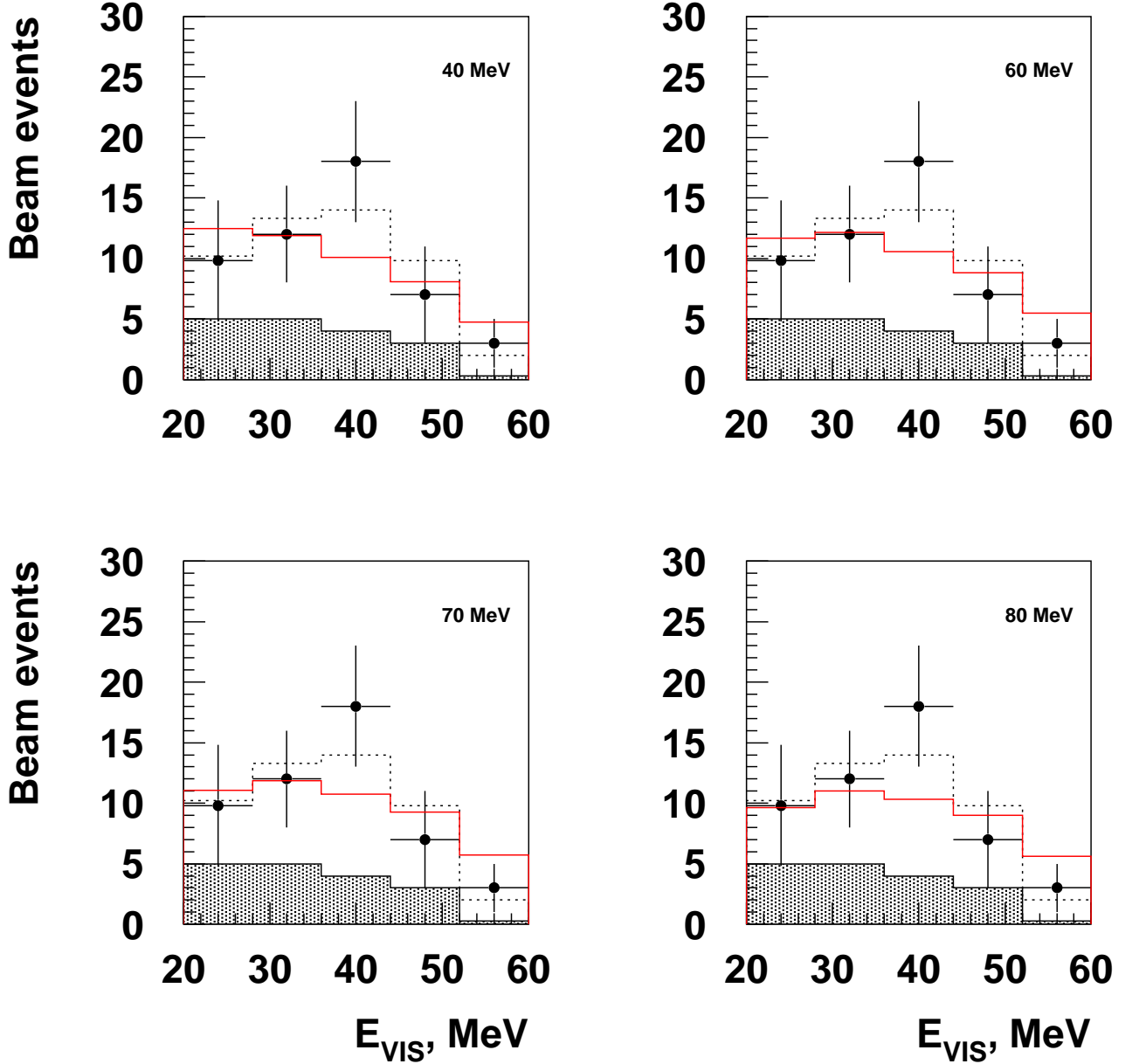


FIG. 9: The same as Fig.8 for Majorana neutrino with $a = 0$.

in this case the neutron energy spectrum becomes softer.

Having this reasonable agreement in mind, we have performed calculations of the LSND ν_μ flux-averaged distributions of the kinetic energy of knockout neutrons produced in the reaction (7). The results are shown in Fig.7 for the ν_h masses of 40 and 80 MeV. The average energy of the recoil neutrons is, respectively, 14 and 16 MeV. To decrease this energy down to the typical energy of neutrons from the reaction $\bar{\nu}_e p \rightarrow e^+ n$ (< 5 MeV) takes about $n_{coll} \simeq 6$ neutron collisions in mineral oil. Taking into account that the average collision length is $L_{coll} \lesssim 10$

cm results in a displacement of the neutron from the primary vertex of the order $\Delta r \simeq L_{coll} \sqrt{n_{coll}} \simeq 25$ cm, which is significantly less than the typical value of $\simeq 70$ cm for the neutrons from the reaction $\bar{\nu}_e p \rightarrow e^+ n$ [3]. Thus, one would expect no significant contribution to the likelihood ratio R_γ due to this effect. The energy decreasing time $\Delta t \simeq \Delta r / \beta c \simeq 5$ ns is also much less than the neutron capture time of $186 \mu s$. As discussed above, the neutrons from the higher energy tail of the distribution shown in Fig. 7 can knock out an additional neutron(s), resulting in observation in LSND of a number of events

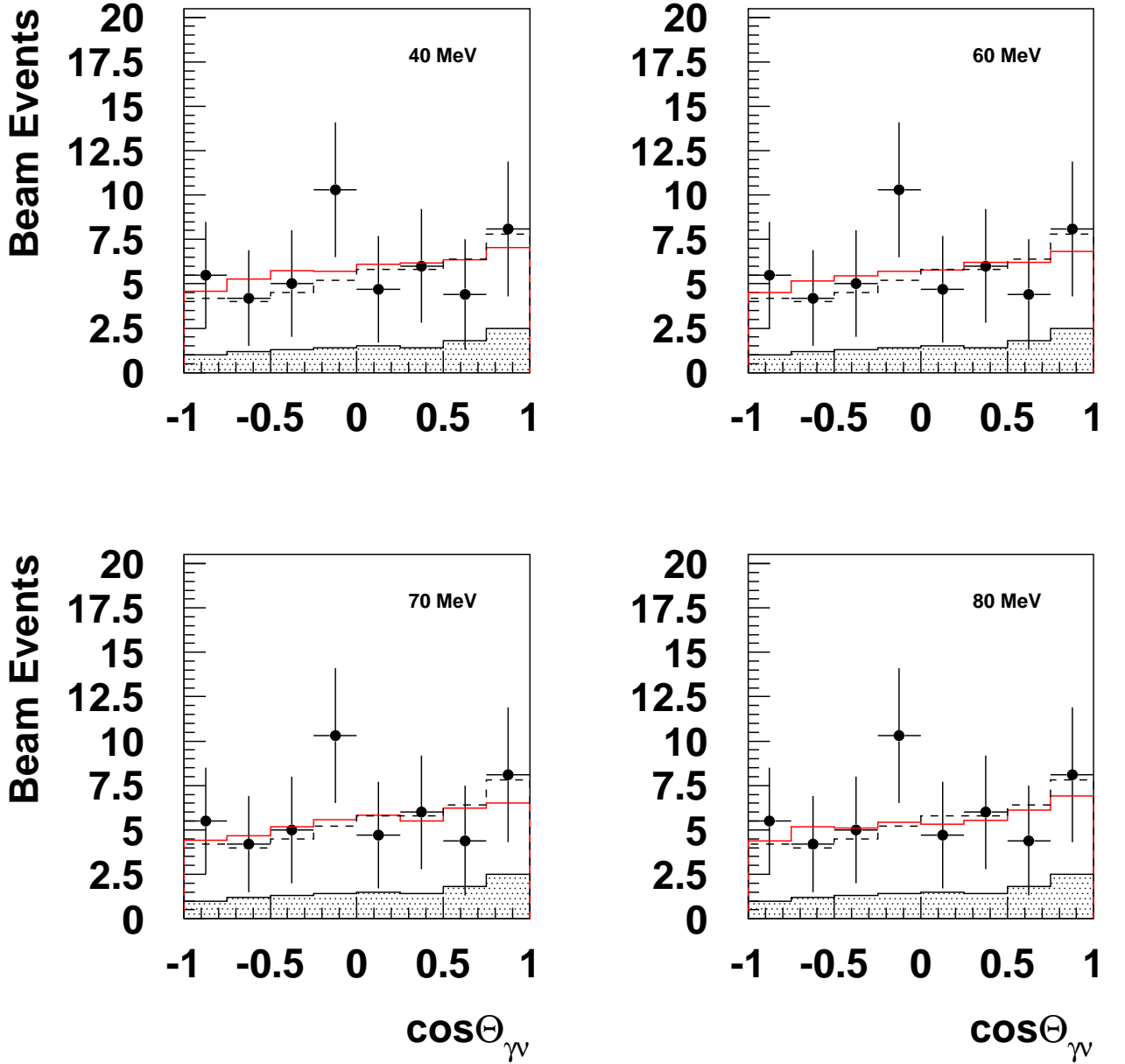


FIG. 10: Distributions of the excess events from the $\nu_h \rightarrow \gamma\nu$ decay reconstructed as $\bar{\nu}_e CC$ events with $36 < E_{vis} < 60$ MeV in the LSND detector as a function of $\cos\Theta$ from the 1993-98 data sample (dots), and a combination of $\nu_h \rightarrow \gamma\nu$ decay of DIRAC sterile neutrino ($a = -1$) plus neutrino background (solid) for different ν_h masses shown in the plots, the mixing strength $|U_{\mu h}|^2 = 10^{-3}$ and the ν_h lifetime $\tau_{\nu_h} = 10^{-9}$ s. A combination of neutrino background plus neutrino oscillations at low Δm^2 (dashed) and the expected distribution from neutrino background (shaded) from Ref. [3] are also shown.

with more than one correlated capture γ 's. To estimate this number, we use the results of the measurement of the neutron yield from the 70 MeV proton beam collisions with the thick graphite target [29], assuming that this yield is approximately the same for the neutron induced reaction of the same energy. The measured number of neutrons per proton is found to be $\simeq 0.06n/p$. The neu-

tron energy threshold to produce a secondary neutron in collisions with ^{12}C nucleus is about 20 MeV. The fraction of neutrons with energy greater than 20 MeV in the distribution shown in Fig.7, is $\simeq 20 - 25\%$ depending on the value of the ν_h mass. Taking into account these results, we find that the total fraction of events with more than one correlated gammas from the flux-averaged re-

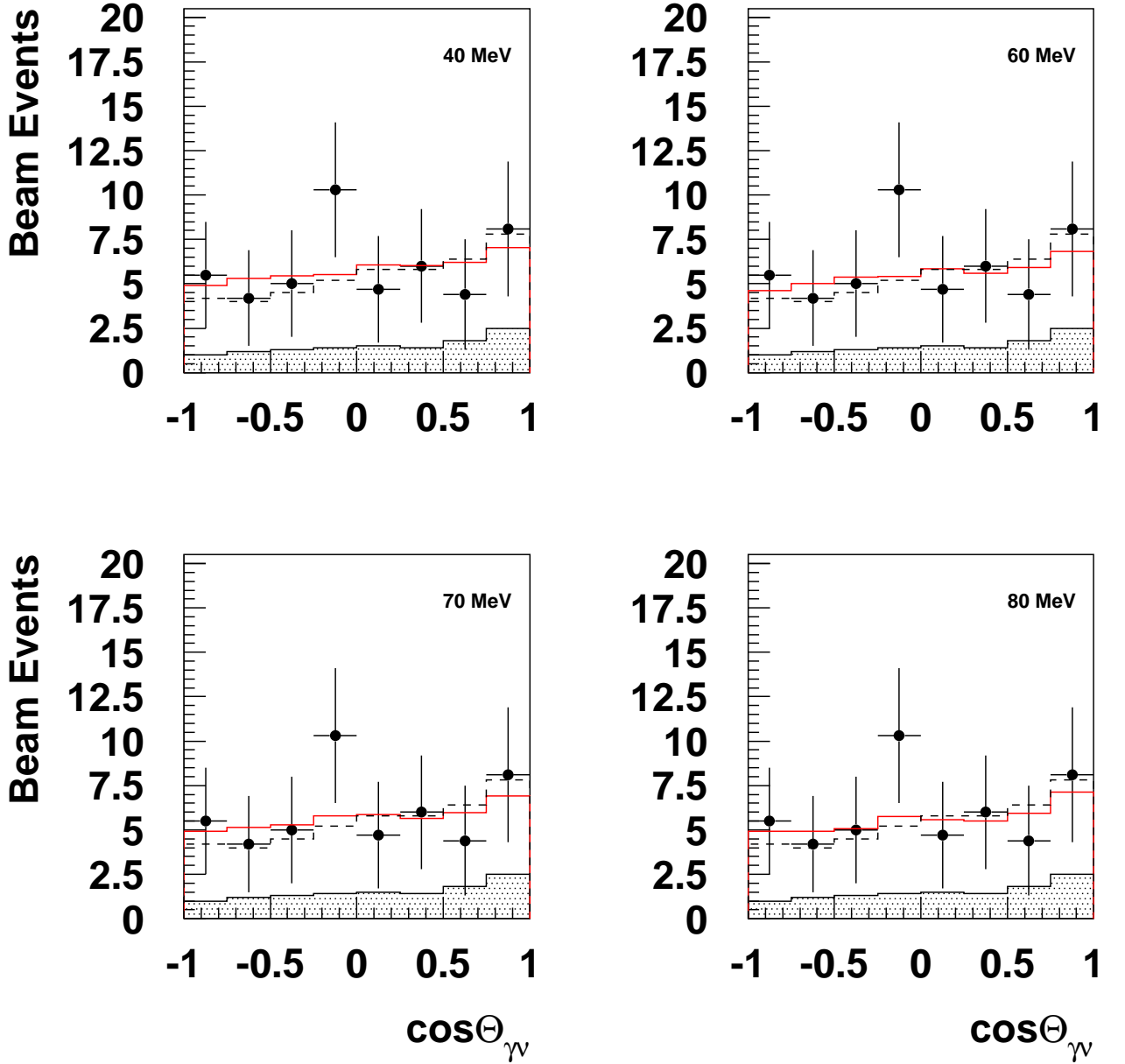


FIG. 11: The same as in Fig.10 for Majorana case with $a = 0$.

action (7) is $\lesssim 2\%$. In addition, our calculations could overestimate the fraction of high energy neutrons. The calculations of the reaction $\bar{\nu}_\mu^{12}\text{C} \rightarrow \mu_\nu^{11}\text{C}$ performed in Ref.[25] show that the cross section and recoil neutron energy spectrum are essentially dependent on details of the ^{12}C level structure for neutron energies below 30 MeV. The consideration of such effect, including the re-scattering of outgoing neutrons, is quite important for the emission spectrum, as it will shift the spectrum to lower neutron energies. Therefore, we may assume, that the fraction of events with > 1 correlated γ is less

then 2%, or 0.6 events. This number should be compared with the background of $\lesssim 5$ such events expected in the LSND experiment at the 2σ level [3]. Thus, our estimate is compatible with the (approximately zero) number of events with > 1 correlated γ 's observed by LSND for the full $20 < E_{vis} < 60$ MeV energy region.

A cross check for the fraction of neutron emitted in the reaction (7) can be obtained from the comparison of results obtained for the inclusive reaction $^{12}\text{C}(\bar{\nu}_\mu, \mu^+ n)X$ in this work, in Ref.[24], and by the LSND collaboration [23]. In this reaction the presence of a muon and a neu-

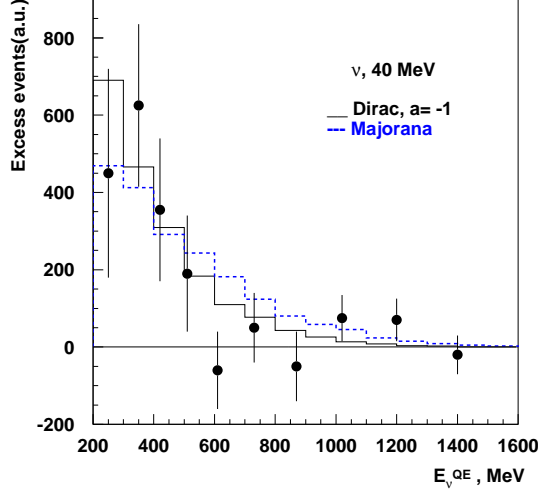


FIG. 12: Distributions of the excess events in the MiniBooNE detector from the $\nu_h \rightarrow \gamma\nu$ decay reconstructed as $\nu_e CC$ events as a function of E_{ν}^{QE} for $|U_{\mu h}|^2 = 3 \times 10^{-3}$, $m_{\nu_h} = 40$ MeV and $\tau_{\nu_h} = 10^{-9}$ s, and for Dirac ($a = -1$, solid), and Majorana ($a = 0$, dashed) cases. The dots are experimental points for the excess events in the MiniBooNE detector. Error bars include both statistical and systematic errors [8]. The comparison of the distributions with the experimental data yields a χ^2 of 7.1 (solid) and 9.3 (dashed) for 8 DF.

tron is established by detection of the Cerenkov ring and of the γ ray from the neutron's capture as described in detail in Ref. [30]. We found that the fraction of events accompanied by the emission of a recoil neutron is $\simeq 81\%$. This number has to be compared with the fractions of 79 % predicted from the calculations in [24], and $(79.6 \pm 40.0)\%$ obtained by LSND [23]. The agreement is quite good.

The total cross section of the reaction $\nu_{\mu}^{12}C \rightarrow \nu_h n X$ for 100% mixing is estimated by extrapolating the available cross section for the reaction $\nu_{\mu}^{12}C \rightarrow \nu_{\mu} n X$ ($\simeq 24 \times 10^{-40}$ cm²) calculated for the incident neutrino energy of 150 MeV [26, 28] to the lower energy region < 150 MeV and by taking into account the phase space suppression factor. Note, the average ν_{μ} energy for the spectrum above the production threshold of the 40 MeV ν_h is 110 MeV, see Fig. 4. The ν_{μ} flux-averaged cross section is found to be $\sigma(\nu_{\mu}^{12}C \rightarrow \nu_h n X) \simeq (16 \pm 6.5) \times 10^{-40}$ cm² for the production of the 40 MeV ν_h with the uncertainty taken to be 40% due to accuracy of the extrapolation procedure.

The visible energy distributions expected from a combination of the $\nu_h \rightarrow \gamma\nu$ events plus neutrino background in the LSND detector [3] calculated for heavy neutrino masses from 40 to 80 MeV are shown in Fig.'s 8,9 for the energy range $20 \lesssim E_{vis} \lesssim 60$ MeV, for Dirac ($a = -1$) and Majorana cases, respectively. The distribution expected from a combination of neutrino background plus

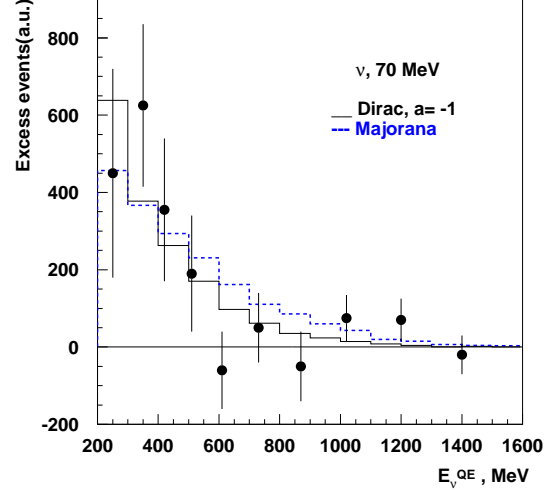


FIG. 13: Same as Fig.14 for the 70 MeV ν_h . The comparison of the distributions with the experimental data yields a χ^2 of 7.5 (solid) and 9.2 (dashed) for 8 DF.

neutrino oscillations at low Δm^2 [3] is also shown for comparison. The clean experimental sample of the oscillation candidate events shown in Fig.'s 8,9 is obtained by enforcing strongly correlated gammas with the cut $R_{\gamma} > 10$. In this case the beam on-off excess is 49.1 ± 9.4 events while the estimated neutrino background is only 16.9 ± 2.3 resulting in the total excess of $32.2 \pm 9.4 \pm 2.3$ events [3].

The distributions for $\cos\Theta_{\gamma\nu}$, cosine of the angle between the incident neutrino and decay photon, for events with $36 \lesssim E_{vis} \lesssim 60$ MeV are shown in Fig.'s 10, 11. The spectra are shown for m_{ν_h} from 40 to 80 MeV and $\tau_{\nu_h} = 10^{-9}$ s. The distributions are obtained assuming that the energy deposited by the decay photon is misreconstructed as the energy from a single electron track. Simulations are in reasonable agreement with the experimental distributions. For instance, for the distribution shown in Fig.8 for $m_{\nu_h} = 40$ MeV, the comparison with the LSND data yields a χ^2 of 3.6 for 3 DF, corresponding to 34% CL. The best fit results suggest that the ν_h mass is in the region $10 \lesssim m_{\nu_h} \lesssim 90$ MeV and the lifetime is $\tau_{\nu_h} \lesssim 10^{-8}$ s. However, to avoid production of ν_h 's in the KARMEN experiment the low mass limit is set to 40 MeV. The mass upper bound is set to 80 MeV because the higher ν_h mass production in LSND is suppressed by the phase space factor and requires large mixing which is already excluded (see discussions below). The simulations showed that the shape of the E_{vis} distribution is sensitive to the choice of the ν_h mass : the higher mass the harder the visible energy spectrum.

Before reporting results on the required mixing strength $|U_{\mu h}|^2$, let us estimate (for the cross check) the number of events expected for $\bar{\nu}_{\mu} \rightarrow \bar{\nu}_e$ oscillations followed by $\bar{\nu}_e p \rightarrow e^+ n$ scattering in the LSND detector.

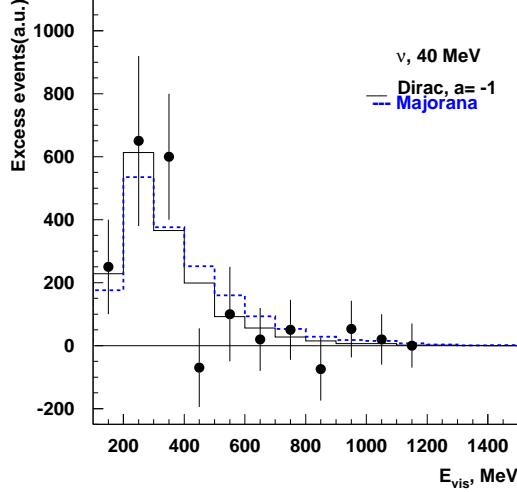


FIG. 14: Distributions of the excess events in the MiniBooNE detector from the $\nu_h \rightarrow \gamma\nu$ decay reconstructed as $\nu_e CC$ events as a function of E_{vis} for $E_\nu^{QE} > 200$ MeV, $|U_{\mu h}|^2 = 3 \times 10^{-3}$, $m_{\nu_h} = 40$ MeV and $\tau_{\nu_h} = 10^{-9}$ s, and for Dirac ($a = -1$, solid), and Majorana ($a=0$, dashed) cases. The dots are experimental points for the excess events in the MiniBooNE detector. Error bars include both statistical and systematic errors [8]. The comparison of the distributions with the experimental data yields a χ^2 of 7.2 (solid) and 9.4 (dashed) for 8 DF.

This number could be estimated as

$$\Delta N_{\bar{\nu}_\mu \rightarrow \bar{\nu}_e} \simeq A \Phi_{\bar{\nu}_\mu} P_{osc} \sigma_{\bar{\nu}_e} f_e \epsilon_e \quad (8)$$

where $A = 7.4 \times 10^{30}$ is the number of free protons in the LSND fiducial volume, $\Phi_{\bar{\nu}_\mu}$ is neutrino flux 1.26×10^{14} ν/cm^2 (see Table 1), averaged over neutrino energy P_{osc} is the $\bar{\nu}_\mu \rightarrow \bar{\nu}_e$ oscillation probability, $\sigma_{\bar{\nu}_e} = 0.95 \times 10^{-40}$ cm^2 is the average cross section over entire energy range, $f_e \simeq 0.89$ is the fraction of events in the energy range $20 < E < 60$ MeV, $\epsilon = 0.42$ is the average positron reconstruction efficiency [3]. Using the above values, we found that the LSND experiment should detect an excess of $\Delta N_{\bar{\nu}_\mu \rightarrow \bar{\nu}_e} \simeq 70$ events if the oscillation probability is $P_{osc} \simeq 2.6 \times 10^{-3}$. This value is in a good agreement with the number of events $87.9 \pm 22.4 \pm 6.0$ quoted in Ref.[3].

Consider now the case of heavy neutrino. The estimate of the mixing parameter $|U_{\mu h}|^2$ was performed by using the following relations. For a given flux of muon neutrinos, Φ_{ν_μ} , the expected number of the $\nu_h \rightarrow \gamma\nu$ decays events in the LSND detector is given by

$$\Delta N_{\nu_h \rightarrow \gamma\nu} \simeq A \int \Phi_{\nu_\mu} \sigma_{\nu_\mu} |U_{\mu h}|^2 f_\gamma f_n f_{phs} P_{dec} P_{conv} \epsilon_\gamma dE \quad (9)$$

where $\Delta N_{\nu_h \rightarrow \gamma\nu} = 32.2 \pm 9.7$ is the number of excess events observed in the 1993-98 data sample (with errors combined in quadrature), $A = 3.7 \times 10^{30}$ is the

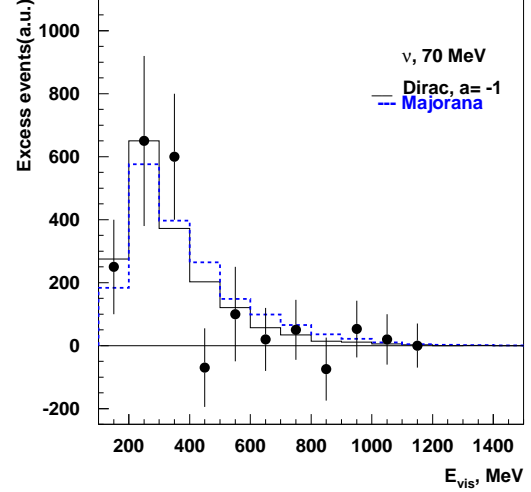


FIG. 15: Same as Fig.14 for the 70 MeV ν_h . The comparison of the distributions with the experimental data yields a χ^2 of 6.8 (solid) and 8.8 (dashed) for 8 DF.

number of carbon nuclear in the LSND fiducial volume, $\sigma_{\nu_\mu n}$ is the cross-section for the reaction $^{12}C(\nu_\mu, \nu_\mu n)X$ with emission of a recoil neutron for the massless case, $f_\gamma \simeq 0.5-0.76$ is the fraction of events in the energy range $20 < E < 60$ MeV, $f_n \simeq 0.4-0.8$ is the fraction of events with emission of a recoil neutron in reaction (7), P_{dec} is the probability for the $\nu_h \rightarrow \gamma\nu$ decay within the detector fiducial volume, P_{conv} is the probability of the decay photon conversion in the detector, and $\epsilon_\gamma \simeq 0.4$ is the overall efficiency for decay photon detection. In Eq.(9) the number of heavy neutrinos produced is proportional to the product of the $^{12}C(\nu_\mu, \nu_\mu n)X$ cross section, the mixing $|U_{\mu h}|^2$ and the phase space factor f_{phs} , which takes into account the threshold effect, due to the heavy neutrino mass. The total ν_μ DIF flux (see Table 1), the number of reconstructed $\bar{\nu}_\mu \rightarrow \bar{\nu}_e$ like [3] and $\nu_\mu CC$ events [23] in the detector were used for cross checks and normalization. The ν_μ flux averaged $^{12}C(\nu_\mu, \nu_\mu n)X$ cross section is $< \sigma(E)_{\nu_\mu n} > \simeq 16 \times 10^{-40}$ cm^2 . The probability of the heavy neutrino to decay radiatively in the fiducial volume at a distance r from the primary vertex is given by

$$P_{dec} = [1 - \exp(\frac{-rm_{\nu_h}}{p_{\nu_h} \tau_{\nu_h}})] \frac{\Gamma(\nu_h \rightarrow \gamma\nu)}{\Gamma_{tot}} \quad (10)$$

where the last term is the branching fraction $Br(\nu_h \rightarrow \gamma\nu) \simeq 1$. Assuming that almost all $\nu_h \rightarrow \gamma\nu$ decays occur inside the fiducial volume of the detector, we estimate the $|U_{\mu h}|^2$ to be in the range

$$|U_{\mu h}|^2 \simeq (2-8) \times 10^{-3}. \quad (11)$$

This result is mainly defined by the uncertainty on the

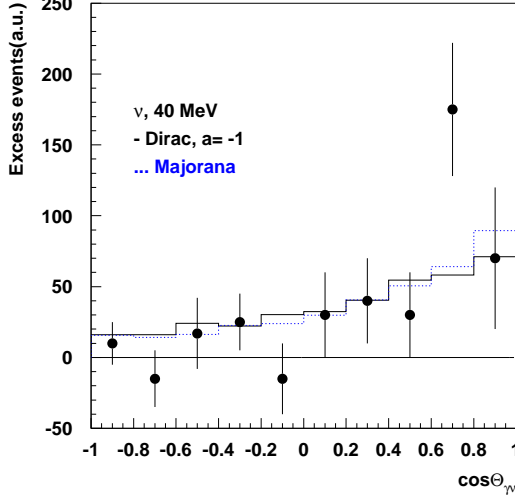


FIG. 16: Distribution of the excess events in the MiniBooNE detector from the ν_h decay reconstructed as $\nu_e CC$ events as a function of $\cos \Theta_{\gamma\nu}$ for $300 < E_\nu^{QE} < 400$ MeV, $|U_{\mu h}|^2 = 3 \times 10^{-3}$, $m_{\nu_h} = 40$ MeV and $\tau_{\nu_h} = 10^{-9}$ s, and for Dirac ($a = -1$, solid), and Majorana ($a = 0$, dashed) cases. The dots are experimental points for the excess events in the MiniBooNE detector. Error bars include both statistical and systematic errors [8]. The comparison of the distributions with the experimental data yields a χ^2 of 10.1(solid) and 9.8(dashed) for 8 DF.

number of excess events and is valid for the mass region

$$40 \lesssim m_{\nu_h} \lesssim 80 \text{ MeV} \quad (12)$$

and the ν_h lifetime

$$\tau_{\nu_h} < 10^{-8} \text{ s} \quad (13)$$

B. The LSND signal of $\nu_\mu \rightarrow \nu_e$ oscillations

During the first three years of LSND data taking, the target area of the LANSCE accelerator consisted of a 30 cm long water target located $\simeq 1$ m upstream of the beam stop. This configuration enhanced the probability of pion decay in flight, allowing LSND to search for $\nu_\mu - \nu_e$ oscillations using ν_μ with energy above 60 MeV. In this case, one expects to observe an excess of events from the reaction $\nu_e^{12}C \rightarrow e^- X$ above the expected backgrounds. This reaction has only one signature (a prompt signal) but the higher energy, the longer track and the directionality of Cherenkov light help improving electron identification and measuring its direction. In this search LSND has observed 40 events to be compared with 12.3 ± 0.9 events from cosmic ray background and 9.6 ± 1.9 events from machine-related (neutrino-induced) processes [31]. The excess of events (18.1 ± 6.6) events corresponds to a $\nu_\mu - \nu_e$ oscillation probability of $(2.6 \pm 1.0) \times 10^{-3}$,

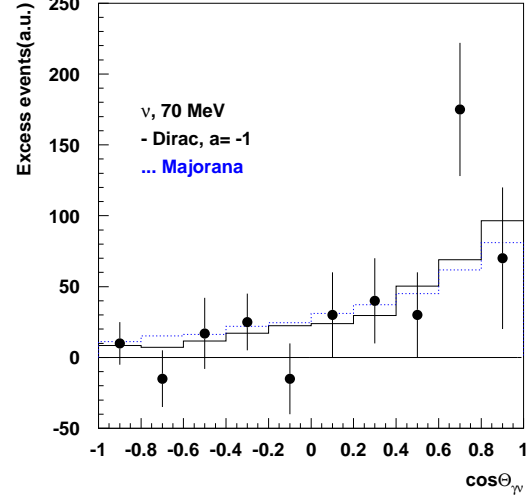


FIG. 17: Same as Fig.16 for the 70 MeV ν_h . The comparison of the distributions with the experimental data yields a χ^2 of 9.3(solid) and 10.1(dashed) for 8 DF.

consistent with the value found from the study of the $\bar{\nu}_e p \rightarrow e^+ n$ reaction below 60 MeV.

The number of the $\nu_h \rightarrow \gamma \nu$ events that would be observed by LSND after applying the high energy cut $E > 60$ MeV, is about (3 – 15) events depending on the ν_h mass and mixing obtained from the combined analysis, as shown below in Sec.V. For example, the number of 15 events corresponds mainly to the reaction $\nu_\mu^{12}C \rightarrow \nu_h X$ occurring on protons, $\simeq 8$ events, which is not expected to produce free neutrons, and on neutrons, in which $\simeq 3$ events have no recoil neutrons, and $\simeq 4$ events are from reaction (7) with a neutron knocked out by the incident neutrino and then identified by the presence of a 2.2 MeV tag photon from the capture on free protons. Thus, for excess events the ratio of the number of events with and without photon tag is $\simeq 4 : 11$ events, which is in an agreement within the errors with the observed corresponding numbers of $(4 \pm 2.5) : (15 \pm 5)$ events in the LSND experiment [31].

IV. THE MINIBOONE ANOMALIES

The MiniBooNE detector is described in details in Ref. [32]. It is using an almost pure ν_μ beam originated from the π^+ decays in flight, which are generated by 8 GeV protons from the FNAL booster. The detector consists of a target, which is a 12.2 m diameter sphere filled with 800 t of mineral oil, surrounded by an outer veto region. The Cherenkov light rings generated by muon, electron and converted photon tracks are used for the reconstruction of the events. The resolutions reached on the vertex position, the outgoing particle direction and the visible energy are 20 cm, 4 degrees and 12%, respectively for

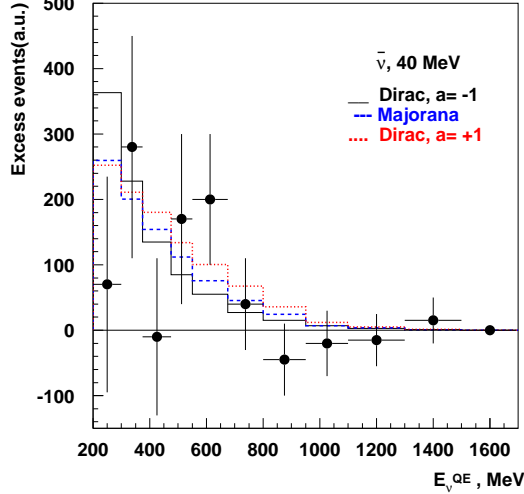


FIG. 18: Distributions of the excess events in the MiniBooNE detector from the $\nu_h \rightarrow \gamma\nu$ decay reconstructed as $\bar{\nu}_e CC$ events as a function of E_ν^{QE} for $|U_{\mu h}|^2 = 3 \times 10^{-3}$, $m_{\nu_h} = 40$ MeV and $\tau_{\nu_h} = 10^{-9}$ s, and for Dirac ($a=-1$, solid and $a=1$, dotted), and Majorana ($a=0$, dashed) cases. The dots are experimental points for the excess events in the MiniBooNE detector. Error bars include both statistical and systematic errors [9]. The comparison of the distributions with the experimental data yields a χ^2 of 8.2 ($a=-1$), 7.1 ($a=0$), 6.7 ($a=1$) for 9 DF. The distribution of the excess events for Dirac case with $a = +1$ is shown for illustrative purpose, see Sec.V.

$CCQE$ electrons [33]. The ν_μ beam is peaked around ~ 600 MeV, has a mean energy of ~ 800 MeV and a high energy tail up to ~ 3 GeV [34].

Below, we consider the MiniBooNE anomalous event excess observed in ν_μ and $\bar{\nu}_\mu$ data and the interpretation of these results in terms of the heavy neutrino decay.

A. Excess of events in ν_μ data

An excess of $\Delta N = 128.8 \pm 20.4 \pm 38.3$ electron-like events has been observed in the data accumulated with 6.64×10^{20} protons on target. For the following discussion several distinctive features of the excess events are of importance [8]: a) the excess is observed for single track events, originating either from an electron, or from a photon converted into a e^+e^- pair with a typical opening angle $\simeq m_e/E_{e^+e^-} < 1$ degree (for $E_{e^+e^-} > 200$ MeV), which is too small to be resolved into two separate Cherenkov rings (here, $m_e, E_{e^+e^-}$ are the electron mass and the e^+e^- pair energy); b) the reconstructed neutrino energy is in the range $200 < E_\nu^{QE} < 475$ MeV, while there is no significant excess for the region $E_\nu^{QE} > 475$ MeV. The variable E_ν^{QE} is calculated under the assumption that the observed electron track originates from a ν_e QE interaction; c) the visible energy E_{vis} is in the

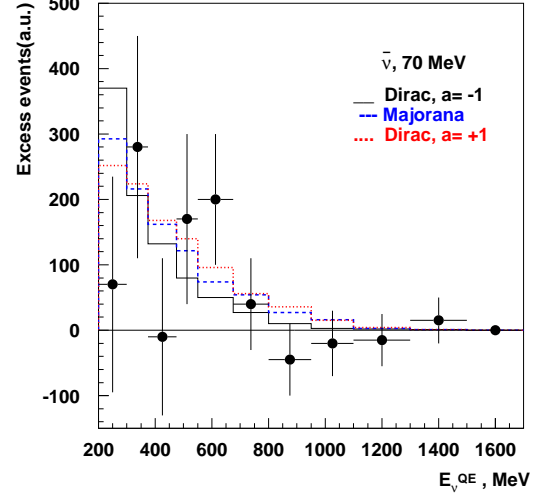


FIG. 19: Same as Fig.18 for the 70 MeV ν_h . The comparison of the distributions with the experimental data yields a χ^2 of 8.3 ($a=-1$), 7.5 ($a=0$) and 6.3 ($a=1$) for 9 DF.

narrow region $200 \lesssim E_{vis} \lesssim 400$ MeV for events with $E_\nu^{QE} > 200$ MeV; d) the angular distribution of the excess events with respect to the incident neutrino direction is wide and consistent with the shape expected from $\nu_e CC$ interactions.

To satisfy the criteria a)-d), we propose that the excess events are originated from the decay of a heavy neutrino ν_h considered in Sec.III. The ν_h 's are produced by mixing in ν_μ neutral-current (NC) QE interactions and deposit their energy via the visible decay mode $\nu_h \rightarrow \nu\gamma$, as shown in Fig.1, with the subsequent conversion of the decay photon into e^+e^- pair in the MiniBooNE target. To make a quantitative estimate, we performed simplified simulations of the production and decay processes shown in Fig.1. In these simulations we used a ν_μ energy spectrum parametrized from the reconstructed $\nu_\mu CCQE$ events [34]. Since in the MiniBooNE experiment the ν_h 's have higher energies and decay over an average distance of $\lesssim 5$ m from the production vertex, the sensitivity in the LSND ν_h mass range of Eq.(12) is restricted to the ν_h lifetimes $\tau_{\nu_h} \lesssim 2 \times 10^{-9}$ s, to be compared with (13).

In Fig.12-17 the distributions of the kinematic variables E_ν^{QE} , E_{vis} and $\cos\Theta_{\gamma\nu}$ for the $\nu_h \rightarrow \nu\gamma$ events are shown for $m_{\nu_h} = 40$ and 70 MeV and $\tau_{\nu_h} = 10^{-9}$ s. These distributions were obtained assuming that the e^+e^- pair from the converted photon is mis-reconstructed as a single track from the $\nu_e QE$ reaction. Simulations are in reasonable agreement with the experimental distributions. For instance, for distributions shown in Fig.12, for Dirac case the comparison with MiniBooNE data yields a χ^2 of 7.1 (7.5) for 8 DF corresponding to 53% ($\simeq 47\%$) CL. for $m_{\nu_h} = 40$ (70) MeV and $\tau_{\nu_h} = 10^{-9}$ s. The simulated excess events, shown in Fig.14,15 are mainly distributed in the narrow region $200 \lesssim E_{vis} \lesssim 400$ MeV. The frac-

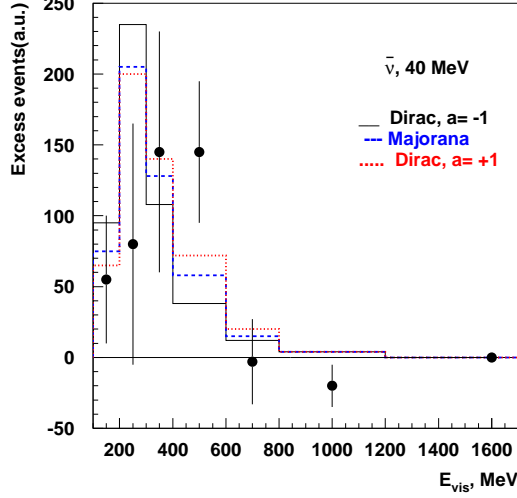


FIG. 20: Distribution of the excess events in the MiniBooNE from the ν_h decay reconstructed as $\bar{\nu}_e CC$ events as a function of E_{vis} for $E_{\nu}^{QE} > 200$ MeV, $|U_{\mu h}|^2 = 3 \times 10^{-3}$, $m_{\nu_h} = 40$ MeV and $\tau_{\nu_h} = 10^{-9}$ s, and for Dirac ($a = -1$, solid and $a = 1$, dotted) and Majorana ($a = 0$, dashed) cases. The dots are experimental points for the excess events in the MiniBooNE detector. Error bars include both statistical and systematic errors [8]. The comparison of the distributions with the experimental data yields a χ^2 of 9.5 ($a = -1$), 7.5 ($a = 0$) and 6.2 ($a = 1$) for 5 DF. The distribution of the excess events for Dirac case with $a = +1$ (dotted) is shown for illustrative purpose, see Sec.V.

tion of events in the region $200 < E_{vis} < 400$ MeV is $\sim 70\%$. The remaining events are distributed over the region $400 \lesssim E_{vis} \lesssim 1200$ MeV, where they can be hidden by the low statistics.

The simulations showed that the shape of the E_{ν}^{QE} and E_{vis} distributions is sensitive to the choice of the ν_h mass: the heavier the ν_h the harder the visible energy spectrum. The best fit results suggest that the ν_h mass is in the region $20 \lesssim m_{\nu_h} \lesssim 600$ MeV and the lifetime is in the range $\tau_{\nu_h} \lesssim 10^{-9} - 10^{-7}$ s, respectively, see also [13].

The estimate of the mixing parameter $|U_{\mu h}|^2$ was performed by using relation similar to Eq.(9). The flux $\Phi(\nu_h)$ was estimated from the expected number of the $\nu_{\mu} NC$ events times the mixing $|U_{\mu h}|^2$, taking into account the phase space factor. The total number of reconstructed $\nu_{\mu} CC$ events in the detector [34] was used for normalization. The probability of the heavy neutrino to decay radiatively in the fiducial volume at a distance r from the primary vertex is given by Eq.(10) assuming the branching fraction $Br(\nu_h \rightarrow \gamma \nu) \simeq 1$. Taking into account the ratio $\nu_{\mu} NCQE / \nu_{\mu} CCQE \sim 0.43$, the number of $\nu_{\mu} CCQE$ events observed [7, 8] and assuming that almost all $\nu_h \rightarrow \gamma \nu$ decays occur inside the fiducial volume of the detector, we estimate the $|U_{\mu h}|^2$ to be in the

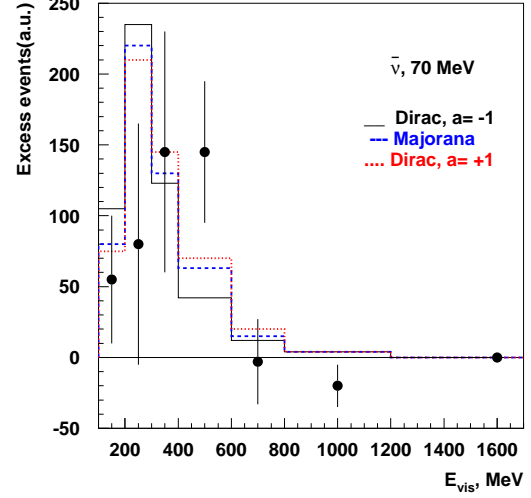


FIG. 21: Same as Fig.20 for the 70 MeV ν_h . The comparison of the distributions with the experimental data yields a χ^2 of 8.5 ($a = -1$), 7.2 ($a = 0$) and 6.4 ($a = 1$) for 5 DF.

range

$$|U_{\mu h}|^2 \simeq (1 - 6) \times 10^{-3}. \quad (14)$$

This result is mainly defined by the uncertainty on the number of excess events. Eq.(14) is also valid for the mass region $40 \lesssim m_{\nu_h} \lesssim 80$ MeV favored by the LSND data.

B. Excess of events in $\bar{\nu}_{\mu}$ data

Recently, the MiniBooNE experiment has reported results from a search for $\bar{\nu}_{\mu} \rightarrow \bar{\nu}_e$ oscillations using a data sample corresponding to 5.66×10^{20} protons on target [9]. An excess of $\Delta N = 43.2 \pm 22.5$ electron-like events is observed which, when constrained by the observed $\bar{\nu}_{\mu}$ events, has a probability for consistency with the background-only hypothesis of 0.5% in the oscillation-sensitive energy range of $475 < E < 1250$ MeV. The data are consistent with $\bar{\nu}_{\mu} \rightarrow \bar{\nu}_e$ oscillations in the 0.1 eV range and with the evidence for antineutrino oscillations from the LSND. Note, that the low statistics antineutrino ($\bar{\nu}_{\mu}$) data collected by the MiniBooNE seem to show no low-energy excess [35].

Similar to the neutrino data [8]: a) the excess is observed for single track events, originating either from an electron, or from a photon converted into a e^+e^- pair; b) the reconstructed neutrino energy is in the wider range $200 < E_{\nu}^{QE} < 700$ MeV, and there is also an excess for the region $E_{\nu}^{QE} > 475$ MeV. The variable E_{ν}^{QE} is calculated under the assumption that the observed electron track originates from a $\bar{\nu}_e$ interaction; c) compare to the ν_{μ} data the visible energy E_{vis} is in the wider

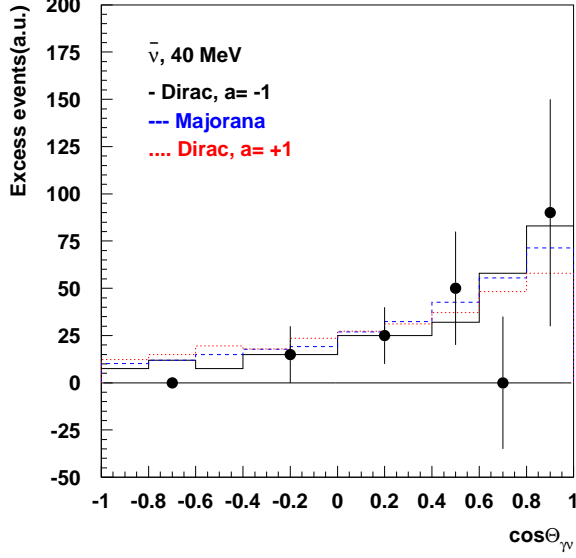


FIG. 22: Distribution of the excess events in the MiniBooNE from the ν_h decay reconstructed as $\bar{\nu}_e CC$ events as a function of $\cos \Theta_{\gamma\nu}$ for $E_{\nu}^{QE} > 200$ MeV, $|U_{\mu h}|^2 = 3.0 \times 10^{-3}$, $m_{\nu_h} = 40$ MeV and $\tau_{\nu_h} = 10^{-9}$ s, and for Dirac ($a = -1$, solid and $a = 1$, dotted), and Majorana ($a = 0$, dashed) cases. The dots are experimental points for the excess events in the MiniBooNE detector. Error bars include both statistical and systematic errors [8]. The comparison of the distributions with the experimental data yields a χ^2 of 3.1 ($a = -1$), 2.7 ($a = 0$) and 3.3 ($a = 1$) for 4 DF. The distribution of the excess events for Dirac case with $a = +1$ (dotted) is shown for illustrative purpose, see Sec.V.

range $200 \lesssim E_{vis} \lesssim 700$ MeV for events with $E_{\nu}^{QE} > 200$ MeV; d) the angular distribution of the excess events with respect to the incident neutrino direction is wide and consistent with the shape expected from $\bar{\nu}_e CC$ interactions. To satisfy the criteria a)-d), we propose again that the $\bar{\nu}_\mu$ excess events are originated from the decay of a heavy neutrino ν_h considered in the previous Sec. The ν_h 's are produced by mixing in $\bar{\nu}_\mu NCQE$ interactions and deposit their energy via the radiative decay mode, as shown in Fig.1, with the subsequent conversion of the decay photon into e^+e^- pair in the MiniBooNE target.

For simulations we used a $\bar{\nu}_\mu$ energy spectrum parametrized from the reconstructed $\bar{\nu}_\mu CCQE$ events [34]. Note, that the antineutrino energy distribution has a maximum at $\simeq 400$ MeV and the average energy of about 600 MeV.

In Fig.18-23 the distributions of the kinematic variables E_{ν}^{QE} , E_{vis} and $\cos \Theta_{\gamma\nu}$ for the $\nu_h \rightarrow \gamma\nu$ events are shown for $m_{\nu_h} = 40$ and 70 MeV and $\tau_{\nu_h} = 10^{-9}$ s. These distributions were obtained assuming that the e^+e^- pair from the converted photon is mis-reconstructed as a single track from the $\bar{\nu}_e QE$ reaction. In this calculation we assume that the angular distribution of photons in the ν_h rest frame has the same asymmetry as for the ν_μ case

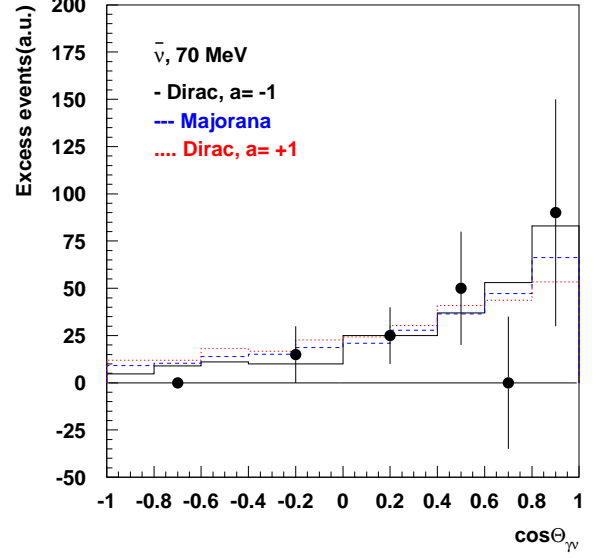


FIG. 23: The same as in Fig.22 for the 70 MeV ν_h . The comparison of the distributions with the experimental data yields a χ^2 of 2.5 ($a = -1$), 2.7 ($a = 0$), and 2.6 ($a = 1$) for 4 DF.

due to the CP conservation, see, Sec.II.

Simulations are in reasonable agreement with the experimental distributions. For instance, for the E_{ν}^{QE} -distributions shown in Fig.18,19, for Dirac case with $a = -1$, the comparison with MiniBooNE data yields a χ^2 of 8.2 (8.3) for 9 DF corresponding to 47% ($\simeq 45\%$) CL. for $m_{\nu_h} = 40(70)$ MeV and $\tau_{\nu_h} = 10^{-9}$ s. The E_{vis} distributions shown in Fig. 20,21 are also in a reasonable agreement with the experiment. For Dirac case with $a = -1$, the comparison with data yields a χ^2 of 9.5 (8.5) for 5 DF corresponding to 10% ($\simeq 14\%$) CL. for $m_{\nu_h} = 40(70)$ MeV and $\tau_{\nu_h} = 10^{-9}$ s. The events are mainly distributed in the region $200 \lesssim E_{vis} \lesssim 600$ MeV, where their fraction is $\sim 90\%$. The remaining events are distributed over the region $600 \lesssim E_{vis} \lesssim 1200$ MeV, where the observed number of excess events is consistent with the expected one.

The analysis of these data within the framework discussed above suggests that the smaller excess of events is observed mainly due to the lower $\bar{\nu}_\mu$ energy and NC cross section. The estimate of the mixing parameter $|U_{\mu h}|^2$ was performed by using relation similar to Eq.(9), assuming the branching fraction $Br(\nu_h \rightarrow \gamma\nu) \simeq 1$. The flux $\Phi(\nu_h)$ was estimated from the expected number of the $\bar{\nu}_\mu NC$ events times the mixing $|U_{\mu h}|^2$, taking into account the phase space factor. The total number of 27,771 reconstructed $\bar{\nu}_\mu CCQE$ events in the detector [9] was used for normalization. Taking into account the ratio $\bar{\nu}_\mu NCQE / \bar{\nu}_\mu CCQE \sim 0.41$, the total number of $\bar{\nu}_\mu CCQE$ events observed and assuming that almost all $\nu_h \rightarrow \gamma\nu$ decays occur inside the fiducial volume of the

detector, we estimate the $|U_{\mu h}|^2$ to be in the range

$$|U_{\mu h}|^2 \simeq (0 - 8) \times 10^{-3}. \quad (15)$$

which is consistent with the mixing from Eq.(11). This result is mainly defined by the uncertainty in the number of excess events. Eq.(15) is valid for the mass region $40 \lesssim m_{\nu_h} \lesssim 600$ MeV, which includes the region favored by the LSND data.

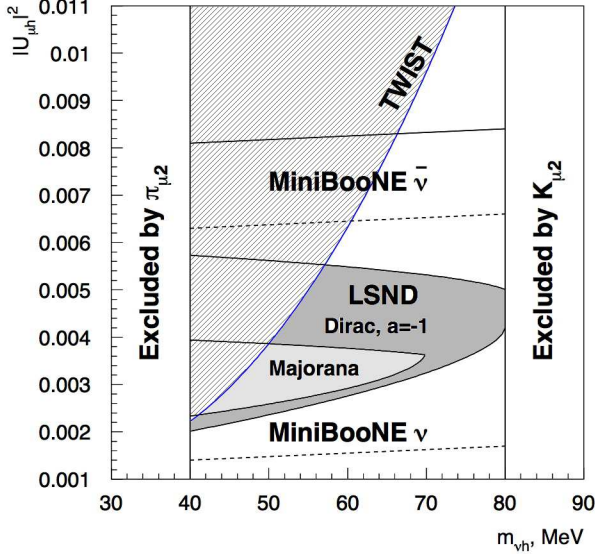


FIG. 24: The 2σ allowed region (dark areas) in the $(m_{\nu_h}; |U_{\mu h}|^2)$ parameter space for Dirac ($a = -1$) and Majorana cases obtained from the combined analysis of LSND and MiniBooNE ν_μ and $\bar{\nu}_\mu$ data. The regions excluded by the $\pi_{\mu 2}$ and $K_{\mu 2}$ decay experiments [36] and allowed bands from MiniBooNE $\bar{\nu}_\mu$ (solid line) and ν_μ (dashed lines) data, are also shown. The hatched region is excluded from the results of precision measurements of the muon decay parameters by the TWIST experiment [37], see Sec. VI.

V. RESULTS FROM THE LSND AND MINIBOONE DATA AND PROPERTIES OF HEAVY NEUTRINO

To obtain the combined regions in the $(m_{\nu_h}; |U_{\mu h}|^2)$ parameter space, we have analyzed both, the LSND and MiniBooNe data simultaneously. The E_{vis} and $\cos\Theta_{\gamma\nu}$ distributions from LSND, and E_ν^{QE} , E_{vis} and $\cos\Theta_{\gamma\nu}$ distributions from MiniBooNE were used for comparison with the corresponding simulated distributions from the $\nu_h \rightarrow \gamma\nu$ decay to constrain the mixing strength and heavy neutrino mass. The shape of the simulated distributions is defined by the mass (and type) of the ν_h , while the mixing strength is defined mainly by the overall normalization of distributions to the number of excess events observed in the experiments. The analysis includes the

following constraints: i) the number of excess events observed; ii) the ν_h lifetime has to be less than 10^{-9} s; iii) the ν_h should be heavier than 40 MeV to avoid its production in the KARMEN experiment; and iv) the number of excess events in the LSND detector in the energy region $60 < E_{vis} < 150$ MeV with a recoil neutron should be $\lesssim 10$ events. The latter constrain came from the upper limit on the number of events observed by LSND in this energy region which are accompanied by > 0 recoil neutrons [31].

The summary results are shown in Fig.24 together with the constraints from the $\pi_{\mu 2}$, $K_{\mu 2}$ experiments and the limit obtained from the recent results of the TWIST experiment on precision measurements of the Michel spectrum in muon decay, see Sec.VI. The size of the MiniBooNE bands for allowed regions from ν_μ and $\bar{\nu}_\mu$ data is also shown. The fit results suggest that the ν_h mass is in the region $40 \lesssim m_{\nu_h} \lesssim 80$ MeV for Dirac ν_h with asymmetry parameter $a = -1$ and in the region $40 \lesssim m_{\nu_h} \lesssim 70$ MeV for Majorana case. The χ^2 contribution from the MiniBooNE ν_μ data is smallest for the whole mass range. As expected, for both cases the main contributions to χ^2 are from the MiniBooNE $\bar{\nu}_\mu$ data. For higher ν_h masses, preferred by the MiniBooNE $\bar{\nu}_\mu$ data, the region of allowed $|U_{\mu h}|^2$ moves towards smaller values, while it is cut by the LSND constrain iv).

The LSND results strongly restrict the allowed ν_h mass region and exclude solutions with $m_{\nu_h} > 80$ MeV, which are favorable by the MiniBooNE $\bar{\nu}_\mu$ data. The analysis gives a 14% χ^2 probability for compatibility between the LSND and MiniBooNE data and the $\nu_h \rightarrow \gamma\nu$ interpretation, demonstrating a reasonable level of agreement.

As already mentioned in Sec. II, the angular and energy distributions of decay photons are sensitive to the type of the heavy neutrino. The analysis shows that better fit results can be obtained provided that the ν_h 's produced in the LSND and MiniBooNe experiments by the muon neutrino decay radiatively as the left-handed Dirac neutrino with asymmetry parameter $a = -1$, while the ν_h 's produced by the muon antineutrinos decay as the right-handed Dirac neutrino with asymmetry parameter $a = +1$. The positive sign of the asymmetry coefficient is strongly preferred by the analysis of MiniBooNE $\bar{\nu}_\mu$ data, while negative sign fit better to the distributions from LSND and MiniBooNE ν_μ data. If the ν_h with such exotic properties exists, that would mean that the $\nu_h \rightarrow \gamma\nu$ decay is not $CP(CPT)$ -conserving [38, 39].

VI. LIMITS ON THE MIXING $|U_{\mu h}|^2$

One may wonder if the mixing strength as large as that of shown in Fig.24 is consistent with the results of previous searches for the ν_h 's. It is well known that heavy neutrino in the mass range $\lesssim 400$ MeV can be effectively probed through the two body decays of charged kaons [14]. The K meson, which is normally decays into a μ and ν_μ , might instead decays into a μ and a ν_h . The experi-

mental signature of the presence of the decay $K^+ \rightarrow \mu \nu_h$ is a peak in the muon energy distribution below the normal one from the ordinary $K_{\mu 2}$ decay at the energy

$$E_\mu = \frac{M_K^2 + m_\mu^2 - m_{\nu_h}^2}{2M_K} \quad (16)$$

The most stringent current experimental limits on $|U_{\mu h}|^2$ for the ν_h mass region below 400 MeV, are summarized in Fig. 25 [36], for a recent review see [40, 41]. One can see, that the limit for the mass region around

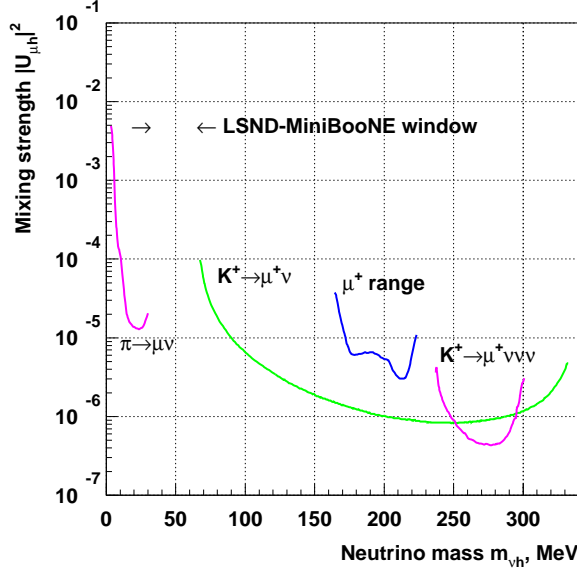


FIG. 25: Bounds on the muonic mixing strength $|U_{\mu h}|^2$ of heavy neutrino vs its mass from $K_{\mu 2}$ range measurements [42], $K^+ \rightarrow \mu^+ \nu \nu \nu$ decay search experiment [43], and from heavy neutrino searches in $\pi \rightarrow \mu \nu$ [44] and $K \rightarrow \mu \nu$ [45] decays. The arrows show the unconstrained LSND-MiniBooNE mass window.

100 MeV, derived from a search for the ν_h at KEK [45], is $|U_{\mu h}|^2 \lesssim 10^{-5}$. Surprisingly, the neighboring $(m_{\nu_h}; |U_{\mu h}|^2)$ region of parameters favorable for the explanation of the LSND and MiniBooNE results remains to be unconstrained. The reason for that is because the ν_h in the mass range of $m_{\nu_h} \simeq 40 - 70$ MeV is outside of the kinematical limits for $\pi_{\mu 2}$ decays and is not accessible in $K_{\mu 2}$ decay experiments due to experimental resolutions and a high background level. For example, to resolve the muon peak of 234 MeV/c from the the 40 MeV ν_h and the main peak of 236 MeV/c, the muon momentum resolution better than 1% is required. Another reason is related to the $K^\pm \rightarrow \mu \nu \gamma$ and $K^+ \rightarrow \mu^+ \pi^0 \nu$ decays which produce a continuous background to the muon momentum distribution below the main peak and essentially constrains the sensitivity of the search for the ν_h mass range $\lesssim 100$ MeV again due to requirement of a very high experimental resolution.

Let us consider this in detail. In the most sensitive experiment performed at KEK [45], degraded K^+ 's were

stopped and decay in the scintillator target. Charged particles from K^+ decays were momentum analyzed by a magnetic spectrometer. To achieve high sensitivity to small signals, the main background decay modes, $K^+ \rightarrow \mu^+ \pi^0 \nu$ and $K^+ \rightarrow \mu^+ \nu \gamma$, were vetoed by using almost hermetic (92% of 4π) low energy threshold ($\simeq 1$ MeV) NaI calorimeter, surrounding the kaon decay target. The veto efficiency for the $K^+ \rightarrow \mu^+ \pi^0 \nu$ decay mode was quite high, better than 99%, because of emission of two photons. While the decay $K^+ \rightarrow \mu^+ \nu \gamma$ was difficult to suppress, and about 30% of photons from this decay mode were undetected. The reasons for that are the following: i) the low energy photons are preferably emitted along the decay muon momentum direction, so they escape undetected; ii) the photo-nuclear absorption cross section is high for photon energies $\simeq 50$ MeV; iii) the absorption of decay photons due to the presence of a dead material in a vicinity of the target. These effects results in a high background level which significantly decreases the sensitivity for the ν_h masses below $\simeq 80$ MeV, as one can see from Fig. 25.

Let us now show that taking into account the dominance of $\nu_h \rightarrow \gamma \nu$ decay and the relatively short ν_h lifetime makes existing experimental bounds even weaker. Indeed, in these searches it was usually assumed that the ν_h is a relatively long lived particle, i.e. $\frac{L m_{\nu_h}}{p_{\nu_h} \tau_{\nu_h}} \ll 1$, where $L \simeq 50$ cm is the typical size of the target region. However, if the decay $\nu_h \rightarrow \gamma \nu$ is dominant and the heavy neutrino is a short lived particle, the ν_h would decay presumably in the vicinity of the target. In this case, the decay photon would generate the veto calorimeter signal, and thus, remain undetected. An estimate shows that for the ν_h lifetime, as short as $\tau_{\nu_h} \lesssim 10^{-9}$ s more than 95% of heavy neutrinos would decay in the target region or inside the calorimeter of the experiment [45] producing a photon with the energy well above the veto energy threshold. Due to this self-veto effect the limit $|U_{\mu h}|^2 \lesssim (2 - 4) \times 10^{-5}$ for the ν_h mass around $\simeq 80$ MeV, could be worsen by more than an order of magnitude, and thus, would be in the region $\simeq 10^{-3}$ close to values from (11). Thus, it would be important to perform an "open mind" search for heavy neutrino in a wider mass range including region around 80 MeV.

If heavy neutrino with the mixing into ν_μ in the range of Eq.(11) exists, it would change the shape of the Michel spectrum relative to the massless case, which is well predicted in the Standard Model(SM). This gives a possibility of using the results of precision measurements of the Michel spectrum in the ordinary muon decay in order to probe possible existence of heavy neutrino. The relatively free of theoretical uncertainties limit on mixing $|U_{\mu h}|^2$ for ν_h masses in the range 30 to 70 MeV was originally set in [47] by using the uncertainty in the parameter $\rho = 0.7518 \pm 0.0026$ obtained from measurements in [48]. The theoretical expression for the mixing of heavy Dirac neutrinos in muon decay with radiative correction included can be found in [46, 47]. Our new limit obtained by using the results of

[47] and the precision measurements of the ρ parameter, $\rho = 0.75014 \pm 0.00017(stat) \pm 0.00044(syst) \pm 0.00011(\eta)$, by the TWIST collaboration [37] is shown in Fig. 24. The limit is obtained by comparing the relative variation of the shape of the Michel spectrum, $\Delta X = \left| \frac{N_{\nu_h} - N_{SM}}{N_{SM}} \right|$, calculated for the massless neutrino case (N_{SM}) with the quoted uncertainties for the ρ parameter by TWIST, and calculated for the spectrum (N_{ν_h}) which includes admixture of the ν_h .

Consider now the sensitivity of neutrino experiments that searched for ν_h 's decaying into e^+e^- pair assuming that these decay mode is dominant [36]. Other decay modes with charged particles in the final state, such e.g. as $\nu_h \rightarrow \mu\pi, \mu\mu\nu, \mu e\nu$ are forbidden by the energy conservation. The direct searches for the $\nu_h \rightarrow \gamma\nu$ decay were performed for the mass region < 1 MeV [36]. The best limit $|U_{\mu h}|^2 \lesssim 10^{-5} - 10^{-6}$ for the mass region $m_{\nu_h} \simeq 40 - 80$ MeV was derived from a search for $\nu_h \rightarrow e^+e^-\nu$ decays in the PS191 beam dump experiment at CERN [49]. It was assumed that these decay modes are dominant and that the ν_h is a relatively long lived particle, i.e. $\frac{L m_{\nu_h}}{p_{\nu_h} \tau_{\nu_h}} \ll 1$, where $L \simeq 1.4 \times 10^2$ m is the distance between the target and the detector. The detector consist of a 12 m long decay volume, 8 chambers to detect charged tracks located inside the volume and followed by a calorimeter. The decay volume was essentially an empty region filled with helium to reduced the number of ordinary neutrino interactions down to $\simeq 100$ events, with the total amount of dead material about 3.6 g/cm². The events searched for in the experiment were requested to consist of two tracks originating from a common vertex in the "vacuum" part of the ν_h decay volume and giving rise to at least one shower in the calorimeter.

Consider now our case, e.g. with $|U_{\mu h}|^2 = 3 \times 10^{-3}$, $m_{\nu_h} = 40$ MeV and the ν_h lifetime $\tau_{\nu_h} = 10^{-9}$ s. Due to the larger mixing the ν_h flux from the K -decays in flight would increase by a factor $\simeq 10^3 - 10^4$. However, several new suppression factors have to taken into account. Firstly, the ν_h flux would decrease by a factor $\simeq 30$ due to the more rapid decay of ν_h 's. Secondly, the experimental signature for the $\nu_h \rightarrow \gamma\nu$ decay would be a e^+e^- pair from the conversion of the decay photon in the decay region. However, the opening angle of the e^+e^- pair is $\simeq m_e/E_{e^+e^-} \lesssim 10^{-3}$ rad, is too small to be resolved in the detector into two separate tracks, and thus the event would be misidentified as a single track event. Such event would be rejected. The rejection factor is estimated to be $\gtrsim 10^{-2}$. Thirdly, the average probability of the photon conversion with the vertex located in the low density decay region (not in a chamber) is as small as $\lesssim 10^{-2}$. Finally, the total number of signal events in PS191 would decrease by a factor more than $\simeq 10^2$ compared to the number of events expected for a long lived ν_h 's produced and decaying through the mixing $|U_{\mu h}|^2 = 10^{-5}$. Note, that the branching fraction for the direct ν_h decay into the $e^+e^-\nu$ final state is $Br(\nu_h \rightarrow e^+e^-\nu) \lesssim 10^{-4}$ [40], assuming the lifetime

$\tau_{\nu_h} \lesssim 10^{-9}$ s and the mixing $|U_{\mu h}|^2 = 3 \times 10^{-3}$, which is also small enough to produce a detectable excess of e^+e^- events in the PS191 experiment. In this estimate the average ν_h momentum is $< p_{\nu_h} > \simeq 4$ GeV, the decay region length is $l = 12$ m and the typical photon energy of $\simeq 2$ GeV [49].

Consider now bounds from LEP experiments [36]. For the mass region around 50 MeV, the model independent limit from the searches for the $Z \rightarrow \nu\nu_h$ decay is $|U_{\mu h}|^2 \lesssim 10^{-2}$, (see e.g. [50]) which is compatible with Eq.(11). Direct searches for radiative decays of an excited neutrino $\nu^* \rightarrow \gamma\nu$ produced in $Z \rightarrow \nu^*\nu$ decays have been also performed [36]. The best limit from ALEPH is [51]

$$Br(Z \rightarrow \nu\nu^*)Br(\nu^* \rightarrow \gamma\nu) < 2.7 \times 10^{-5}. \quad (17)$$

As the experimental signatures for the $\nu^* \rightarrow \gamma\nu$ and $\nu_h \rightarrow \gamma\nu$ decays are the same, we will use this bound for comparison. The number of expected $\nu_h \rightarrow \gamma\nu$ events in ALEPH is proportional to $Br(Z \rightarrow \nu\nu_h)Br(\nu_h \rightarrow \gamma\nu)[1 - \exp(-\frac{lm_{\nu_h}}{p_{\nu_h}\tau_{\nu_h}})]$, with $l \simeq 1$ m and $p_{\nu_h} \simeq 45$ GeV. Taking into account $\frac{Br(Z \rightarrow \nu\nu_h)}{Br(Z \rightarrow \nu\nu)} \simeq |U_{\mu h}|^2$ and using (17), we find

$$|U_{\mu h}|^2 \times \frac{m_{\nu_h} [MeV]}{\tau_{\nu_h} [s]} < 4.8 \times 10^9. \quad (18)$$

Using Eq.(11) results for the mass range (12) in

$$\tau_{\nu_h} \gtrsim 10^{-11} - 10^{-10} \text{ s}, \quad (19)$$

which is consistent with (13).

VII. PROPOSED SEARCHES FOR HEAVY NEUTRINO

In this section we consider proposed searches for heavy neutrinos in $K_{\mu 2}$ decays and neutrino experiments.

A. Search for the ν_h in K decays

As discussed in Sec. VI, the existence of heavy neutrinos with the masses $\lesssim 400$ MeV can be effectively probed by searching for a peak from the ν_h in two body $K^+ \rightarrow \mu\nu_\mu$ decays of charged kaons [14]. Depending on the experimental method, one could also search for a peak in the missing mass distribution corresponding to the mass of the heavy neutrino. The number of $K^+ \rightarrow \mu\nu_h$ events in the peak is defined by the mixing factor $|U_{\mu h}|^2$ as well as a phase space factor depending on the ν_h mass [14]. For the mass interval $m_{\nu_h} \simeq 40 - 80$ MeV the chirality-flip is mostly due to sterile neutrino mass which results in

$$\Gamma(K \rightarrow \mu\nu_h) \approx \Gamma(K \rightarrow \mu\nu_\mu)|U_{\mu h}|^2 \left(\frac{m_{\nu_h}}{m_\mu} \right)^2. \quad (20)$$

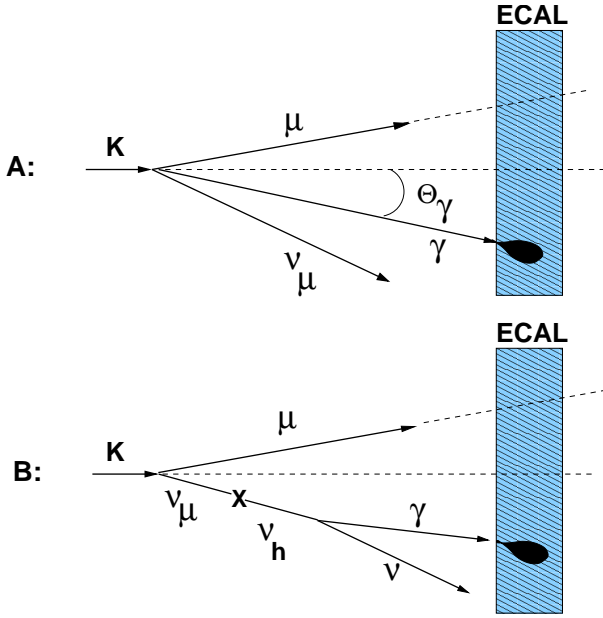


FIG. 26: Schematic illustration of an experiment to search for radiative neutrino decay in $K_{\mu 2}$ decays in flight at high energies. A: for the (relatively) long-lived ν_h , photons from the background decay $K \rightarrow \mu \nu \gamma$ are detected in the electromagnetic calorimeter (ECAL) with a high efficiency due to the Lorentz boost; B: for the short-lived ν_h the photon from the $\nu_h \rightarrow \gamma \nu$ decay is also detected. See text.

Using Eq. (11), we find that the branching fraction of $K \rightarrow \mu \nu_h$ is in the experimentally accessible range:

$$Br(K \rightarrow \mu \nu_h) \approx 10^{-4} - 10^{-3} \quad (21)$$

for heavy neutrino masses in the range 40 - 80 MeV. There are two advantages to search for the ν_h in the K decays. Namely, i) the expected number of signal events occurring in a detector is $\propto |U_{\mu h}|^2$, as follows from (20). While in neutrino scattering experiments the ν_h decay signal rate is proportional to $\propto |U_{\mu h}|^4$, and, thus is more suppressed (the mixing $|U_{\mu h}|^2$ appears twice, through the heavy neutrino production, and through its decays in the detector); ii) the observation of peaks in the muon and/or the missing mass spectra gives unambiguous signature for the existence of heavy neutrino.

As discussed in Sec.VI, the major physics background to the experiments searching for the ν_h peak in $K_{\mu 2}$ decays at rest is the radiative kaon decay $K^+ \rightarrow \mu \nu \gamma$ which has the branching fraction of about 1 % for the photon energy above 10 MeV [36]. This background results in an admixture of a continuous spectrum to the muon momentum distribution below the main peak and essentially constrains the sensitivity of the search for the ν_h mass range $\lesssim 100$ MeV. To improve sensitivity this background decay mode has to be suppressed by increasing the detection efficiency of the decay photons. Experimentally, improvement of the photon efficiency for the searches with the K decays at rest is difficult due to lim-

itation factors discussed in Sec.VI.

Here, we propose to use K decays in flight in order to improve sensitivity against this background source. A substantial increase in the detection efficiency of radiative photons could be obtained by using the K decays in flight at high energies. In this case, the vast majority of decay photons would be within the geometrical acceptance of a detector because they are distributed within a narrow cone with the maximal photon angle of the order $\Theta_\gamma \simeq m_K/E_K \simeq 7$ mrad for the kaon energy of $E_K = 70$ GeV, as schematically illustrated in Fig. 26A. Thus, the detection efficiency of high energy decay photons from the decay $K^+ \rightarrow \mu^+ \nu \gamma$ in an electromagnetic calorimeter is expected to be almost 100%. If the ν_h is a relatively long-lived particle, with the lifetime $\gtrsim 10^{-10}$ s, then it would rarely decay in the experiment, as the ν_h average decay length of $\simeq 300$ m is much bigger than the typical length of a decay volume $\simeq 100$ m. The detection of a muon and a photon in the final state would unambiguously signal the detection of the radiative K decay, as shown in Fig. 26A, or another background decay mode. This would reduce the background significantly and allow the measurements of the muon energy distribution with a higher sensitivity. If the ν_h is a short-lived, with the lifetime $\simeq 10^{-11}$ (see Eq.(19)) and corresponding ν_h decay length of about 30 m, then detection of a muon and a photon in the final state would mean either detection of a background process or detection of the signal from the decay $\nu_h \rightarrow \gamma \nu$, as shown in Fig. 26B. In this case, one could still suppress the background by rejection of the $\mu \gamma$ observed events at a cost of the signal efficiency reduction. To avoid this reduction, one could try to identify signal events by using the fact that the observed photon is originated from a secondary vertex, which is displaced from the primary one at a large distance, provided precise measurements of the photon directionality can be performed.

A good example of the experiment where the proposed search could be performed is the NA-62 at CERN [52]. The experiment is running at kaon energy of 74 GeV. The detector is well equipped to identify and measure the momenta/energy and directions of the charged particles. The photons are precisely measured with a LXe electromagnetic calorimeter (ECAL), and could be detected with almost 100% efficiency provided the central ECAL beam hole is replaced by an active photon detector. Other experiments capable to search for the $\nu_h \rightarrow \gamma \nu$ decay with existing data are the E787 and its upgrade E949, searching for $K \rightarrow \nu \nu$ decay at BNL [53]. The experiment is equipped with the almost 4π veto electromagnetic calorimeter allowing good rejection of photons from background $K^+ \rightarrow \mu^+ \pi^0 \nu$ and $K^+ \rightarrow \mu^+ \nu \gamma$ decays.

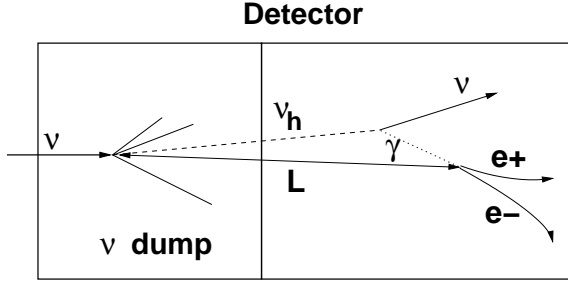


FIG. 27: Schematic illustration of the proposed neutrino experiment to search for radiative neutrino decay in $\nu_\mu NC$ interactions. The electromagnetic and hadronic secondaries from the $\nu_\mu NC$ event are absorbed in the initial part of a neutrino detector served as a dump. Heavy neutrino produced through muonic mixing, see Fig.1, penetrates the dump and decay into a photon and a light neutrino in the downstream decay region of the detector. The experimental signature of the $\nu_h \rightarrow \gamma\nu$ decay is appearance of a single high energy e^+e^- pair from the conversion of the decay photon at a distance L from the primary vertex significantly larger than the detector nuclear interaction length $L \gg \lambda_0$. Precise identification of the electromagnetic nature of the excess events is crucial for this experiment.

B. Search for the decay $\nu_h \rightarrow \gamma\nu$ in neutrino interactions

The main idea of the proposed experiment to search for radiative neutrino decay in $\nu_\mu NC$ interactions is illustrated in Fig. 27. A neutrino detector is subdivided into two parts, an absorber and a second decay region for detection of converted photons from the decay $\nu_h \rightarrow \gamma\nu$. The secondary particles from $\nu_\mu NC$ interactions occurred in the detector are absorbed in the initial part served as a dump. Heavy neutrinos produced through the muonic mixing penetrate the dump and decay into a photon and a light neutrino in the second downstream part of the detector, with the subsequent photon conversion. The experimental signature of the decay $\nu_h \rightarrow \gamma\nu$ is the appearance of a single e^+e^- pair originating from a secondary vertex displaced from the primary one at a distance L significantly larger than the detector nuclear interaction length $L \gg \lambda_0$. The main background sources are expected from the neutron interactions and K_L decays misidentified as a single photon event. The suppression of these backgrounds can be achieved by increasing the length L , and hence the n, K_L absorption in the downstream part of the detector and by precise identification of the electromagnetic nature of the signal event, which is of great importance for this search.

The almost ideal detector to search for the decay $\nu_h \rightarrow \gamma\nu$ is a detector similar to NOMAD [54]. The NOMAD is equipped with the forward calorimeter (FCAL), where the secondaries from high energy neutrino interactions in FCAL could be dump. In addition it has excellent capability for identification and reconstruction of

converted photons due to the low mass target located in a magnetic field. An example of the reconstruction of two conversion e^+e^- pairs from the decay $\pi^0 \rightarrow 2\gamma$ can be found in Ref.[55]. Some disadvantage of the detector is the short length of the tracking part. The overall detection efficiency of the ν_h production, decay in flight with the subsequent conversion of decay photons into e^+e^- pair and the reconstruction of the conversion pairs is expected to be low.

Another experiment capable to search for the decay $\nu_h \rightarrow \gamma\nu$ is the ICARUS T600 currently taking data at the CERN-Gran Sasso neutrino beam [56]. The detector is composed of two identical adjacent T300 half-modules filled with Liquid Argon (LAr). The detail description of the apparatus can be found in [56]. Each T300 half-module has the following internal dimensions: $3.6m \times 3.9m \times 19.9m$ (length). LAr has a radiation length of $X_0 = 14$ cm and a nuclear interaction length of $\lambda_0 = 83.6$ cm, and therefore provide good electromagnetic and hadronic secondaries absorption and detection capabilities for the proposed search assuming that the length of the decay region is $L \gtrsim 10\text{ m} \gg X_0, \lambda_0$.

The number of $\nu_h \rightarrow \gamma\nu$ events in ICARUS can be estimated as follows

$$N(\nu_h \rightarrow \gamma\nu) \simeq \Delta N_{NC} |U_{\mu h}|^2 P_{dec} P_{det} \epsilon \quad (22)$$

where $N_{NC} \simeq 10^3$ is the number of the detected neutral current events, and $P_{dec} (\simeq 0.4)$, $P_{conv} (\simeq 1)$, $\epsilon (\simeq 0.7)$ are the probabilities for the ν_h decay in the detector fiducial volume and decay photon conversion, and the overall detection efficiency of the e^+e^- pair, respectively. In this estimate the average ν_h momentum is $\langle p_{\nu_h} \rangle \simeq 10$ GeV, $\tau_{\nu_h} \lesssim 10^{-9}$, and the length of the decay region $L = 12$ m. Finally, we find that the number of the expected $\nu_h \rightarrow \gamma\nu$ signal events in ICARUS is

$$\Delta N_{\nu_h \rightarrow \gamma\nu} \simeq 6 \times 10^2 \times |U_{\mu h}|^2 \quad (23)$$

For the allowed mixing, see Fig. 24, this results in $\Delta N_{\nu_h \rightarrow \gamma\nu} \simeq 1 - 3$ events. In case of non-observation, ICARUS could provide a limit for the mixing strength of the order $|U_{\mu h}|^2 \lesssim 10^{-3}$ which is competitive for the mass range 40-80 MeV with the bounds obtained from the TWIST experiment.

Note, the search for an excess of the ν_h decay events can be also performed in the recently proposed ICARUS-like experiment at CERN PS [57], or at FNAL with neutrino detectors such as MicroBooNE [58], HiResM ν [59] and BooNE (a MiniBooNE near detector) [60].

VIII. A MODEL FOR RADIATIVE NEUTRINO DECAYS

The most natural way to allow the radiative decay of the Dirac or Majorana ν_h is to introduce a nonzero transition magnetic moment between the ν_h and the light neutrino ν , see e.g. [16, 17]. The non-zero magnetic moment of neutrino, although tiny, is predicted even in the

Standard Model (SM). Its value is typically proportional to the ν_h mass. In many extensions of the SM. Thus, the intention to include a large transition magnetic moment, which is responsible for the prompt radiative decay of the $\lesssim 100$ MeV ν_h is not particularly exotic from a theoretical viewpoint.

The ν_h lifetime due to a transition moment μ_{tr} is given by [16]

$$\tau_{\nu\gamma}^{-1} = \frac{\alpha}{8} \left(\frac{\mu_{tr}}{\mu_B} \right)^2 \left(\frac{m_{\nu_h}}{m_e} \right)^2 m_{\nu_h} \quad (24)$$

The requirement for the $\nu_h \rightarrow \gamma\nu$ decays to occur mostly inside the MiniBooNE fiducial volume results in

$$\tau_{\nu\gamma} < 10^{-9} \text{ s} \quad (25)$$

and

$$\mu_{tr} > 3.7 \times 10^{-8} \mu_B. \quad (26)$$

The total ν_h decay width is $\Gamma_{tot} = \Gamma(\nu_h \rightarrow \nu\gamma) + \Gamma(\nu_h \rightarrow \nu e^+ e^-)$, where $\Gamma(\nu_h \rightarrow \nu\gamma)$ is the $\nu_h \rightarrow \gamma\nu$ decay rate, and $\Gamma(\nu_h \rightarrow \nu e^+ e^-)$ is the decay rate into $e^+ e^-$ pair which is proportional to the square of the mixing $|U_{\mu h}|^2$. The calculations of these rates can be found, e.g. in [40]. For $m_{\nu_h} \simeq 40-80$ MeV and $\mu_{tr} > 10^{-8} \mu_B$, we found that the radiative decay is dominant, $Br(\nu_h \rightarrow \gamma\nu) > 0.9$. For example, for $\mu_{tr} = 3.7 \times 10^{-8} \mu_B$ and $|U_{\mu h}|^2 = 10^{-3} - 10^{-2}$, the expected ratio of decay rates for $\nu e^+ e^- : \gamma\nu < 10^{-3}$. Radiative neutrino decay has been searched for in accelerator and reactor experiments for the neutrino mass less than 1 MeV [36]. None of the neutrino experiments has reported a bound on the mixing strength $|U_{\mu h}|^2$ or on the combination $|U_{\mu h}|^2 \mu_{tr}$, for the radiative neutrino decay in the mass region 40-80 MeV.

The mixing $|U_{\mu h}|^2$ would result in a contribution to the effective ν_μ magnetic moment, $\mu_{\nu_\mu}^{eff} \simeq |U_{\mu h}|^2 \mu_{tr} \simeq (0.4 - 4.0) \times 10^{-10} \mu_B$, due to the non-zero ν_h magnetic moment. This contribution is below than the best direct LSND experimental limit derived from the muon neutrino-electron scattering $\mu_{\nu_\mu}^{eff} < 6.8 \times 10^{-10} \mu_B$ [61]. Note, however, that in this particular case the LSND limit is not directly applicable to the ν_h magnetic moment as the limit was obtained for the DAR $\bar{\nu}_\mu$, which, as discussed in Sec. II, cannot produce ν_h in the LSND experiment due to its heavy mass.

Consider now again bounds from LEP experiments [36]. For the mass region around 50 MeV, the model independent limit from the searches for the $Z \rightarrow \nu\nu_h$ decay is $|U_{\mu h}|^2 \lesssim 10^{-2}$, (see e.g. [50]) which is compatible with Eq.(11). Consider the constrain (17) from direct searches for radiative decays of an excited neutrino $\nu^* \rightarrow \gamma\nu$ produced in $Z \rightarrow \nu^* \nu$ decays [51].

The number of expected $\nu_h \rightarrow \gamma\nu$ events in ALEPH is proportional to $Br(Z \rightarrow \nu\nu_h) Br(\nu_h \rightarrow \gamma\nu) [1 - \exp(-\frac{l m_{\nu_h}}{p_{\nu_h} \tau_{\nu_h}})]$, with $l \simeq 1$ m and $p_{\nu_h} \simeq 45$ GeV. Taking into account $\frac{Br(Z \rightarrow \nu\nu_h)}{Br(Z \rightarrow \nu\nu)} \simeq |U_{\mu h}|^2$ and using Eq.(24),

we find

$$|U_{\mu h}|^2 \times \left(\frac{\mu_{tr}}{\mu_B} \right)^2 < 1.9 \times 10^{-16}. \quad (27)$$

Using Eq.(11) results in $\mu_{tr} \lesssim (2.6 - 1.4) \times 10^{-7} \mu_B$, which is consistent with Eq.(26).

The limit on the μ_{tr} between the ν_h and the ν_μ has been obtained in Ref.[62], based on the idea of the Primakoff conversion $\nu_\mu Z \rightarrow \nu_h Z$ of the muon neutrino into a heavy neutrino in the external Coulomb field of a nucleus Z , with the subsequent $\nu_h \rightarrow \gamma\nu$ decay. By using the results from the NOMAD experiment [54, 63], a model-independent bound $\mu_{tr}^{\mu h} \lesssim 4.2 \times 10^{-8} \mu_B$ was set for the ν_h masses around 50 MeV (see Table 1 and Fig.2 in Ref.[62]), which is also consistent with Eq.(26). Values of μ_{tr} larger than $10^{-8} \mu_B$ for the $m_{\nu_h} > 40$ MeV could be obtained e.g. in the framework of the Zee model [16].

IX. SUMMARY

In summary, we reexamine neutrino oscillation results from the accelerator experiments LSND, KARMEN and MiniBooNE. We show that the LSND evidence for $\bar{\nu}_\mu \rightarrow \bar{\nu}_e$ oscillations, its long-standing disagreement with the results from KARMEN, and the anomalous event excess observed by MiniBooNE in ν_μ and $\bar{\nu}_\mu$ data can be explained by the production and decay of a heavy sterile neutrino. The shape of the excess events in several kinematic variables in the LSND and MiniBooNE ν_μ and $\bar{\nu}_\mu$ data is found to be consistent with the distributions obtained within this interpretation, assuming that ν_h 's are created by mixing in ν_μ neutral-current interactions and decay promptly into a photon and a light neutrino. Therefore, our main prediction is that the excess of events observed in the LSND and MiniBooNE experiments originates from the COMPTON scattering or $e^+ e^-$ conversion of the decay photons in these detectors. Therefore, any confirmation of the photon origin of the excess events by measurements with a detector able to distinguish electrons and photons would be crucial for this explanation.

The combined analysis of the energy and angular distributions of the excess events observed in the LSND and MiniBooNE detectors suggests that the required $(m_{\nu_h}; |U_{\mu h}|^2)$ parameter region corresponds to the masses of $m_{\nu_h} \simeq 40 - 70$ MeV and the mixing strength of $|U_{\mu h}|^2 \simeq 10^{-3} - 10^{-2}$ for the ν_h lifetime $\tau_{\nu_h} \lesssim 10^{-9}$ s. Surprisingly, this LSND-MiniBooNE parameters window is found to be unconstrained by the results from the most sensitive $K_{\mu 2}$ and neutrino experiments. A new limit on $|U_{\mu h}|^2$ for neutrino masses in the range 40 to 80 MeV is set from the precision measurements of the Michel spectrum by the TWIST experiment. The question of whether the ν_h is Dirac or Majorana neutrino is discussed. The better fit results could be obtained provided that the ν_h created in $\nu_\mu NC$ interactions decay radiatively as a left-handed Dirac particle, while being

created in $\bar{\nu}_\mu NC$ interactions decays as a right-handed Dirac neutrino.

We also discuss the most natural model for the decay $\nu_h \rightarrow \gamma \nu$ based on the non-zero transition magnetic moment between the ν_h and the light neutrino. We show that the mixing strength of $|U_{\mu h}|^2 \simeq 10^{-3} - 10^{-2}$ and the required magnetic moment of $\mu_{tr} \gtrsim 10^{-8} \mu_B$ are compatible with the bounds from the previous experiments. Finally, note that a short ν_h lifetime is necessary to avoid the constraints coming from cosmological and astrophysical considerations [64].

The results obtained provide strong motivation for a sensitive search for the ν_h in a near future K decay or neutrino experiments, which fit well in the existing/planned experimental programs at CERN or FNAL. We note that an analysis of the excess of events due to the $\nu_h \rightarrow \gamma \nu$ decay may also be possible with existing

neutrino data, e.g. new results could be obtained with the NOMAD detector [54].

The analysis gives an estimate for the parameters $|U_{\mu h}|^2$ and m_{ν_h} and may be improved by more accurate and detailed simulations of the LSND and MiniBooNE detectors, which are beyond the scope of this work.

Acknowledgments

I would like to thank L. Camilleri, D.S. Gorbunov, N.V. Krasnikov, S.A. Kulagin, L. Di Lella, V.A. Matveev, V.A. Rubakov, and A. Rubbia for discussions. I am grateful to W.C. Louis for comments and clarifications, and to D. Sillou for help in manuscript preparation.

-
- [1] Liquid Scintillator Neutrino Detector at the Los Alamos Neutron Science Center.
 - [2] C. Athanassopoulos et al., Phys. Rev. Lett. **77**, 3082 (1996); C. Athanassopoulos et al., Phys. Rev. C **54**, 2685 (1996); C. Athanassopoulos et al., Phys. Rev. Lett. **81**, 1774 (1998).
 - [3] A. Aguilar et al., Phys. Rev. D **64**, 112007(2001).
 - [4] Karlsruhe-Rutherford Medium Energy Neutrino experiments at the Rutherford-Appleton Laboratory.
 - [5] G. Drexlin et al., Nucl. Instr. Meth. **A 289**, 490 (1990).
 - [6] Booster Neutrino Experiment at Fermilab
 - [7] A.A. Aguilar-Arevalo et al., Phys. Rev. Lett. **98**, 231801 (2007).
 - [8] A.A. Aguilar-Arevalo et al., Phys. Rev. Lett. **102**, 101802 (2009) ; arXiv:0812.2243.
 - [9] A.A. Aguilar-Arevalo et al., arXiv:1007.1150 [hep-ex] .
 - [10] C. Athanassopoulos et al., Phys. Rev. C **55**, 2078 (1997).
 - [11] G. Drexlin et al., Phys. Lett. **B 267**, 321 (1991).
 - [12] See, for example, T. Schwetz, Pramana **72**, 119 (2009).
 - [13] S.N. Gninenko, Phys. Rev. Lett. **103**, 241802 (2009); arXiv:0902.3802 [hep-ph].
 - [14] R.E. Shrock, Phys. Rev. D **24**, 1232 (1981); R.E. Shrock, Phys. Rev. D **24**, 1275 (1981).
 - [15] S.N. Gninenko and D.S. Gorbunov, Phys. Rev. D **81**, 075013 (2010); arXiv:0907.4666 [hep-ph].
 - [16] See for example, R.N. Mohapatra and P.B. Pal, "Massive Neutrinos in Physics and Astrophysics", World Scientific, Singapore, 1991.
 - [17] F. Boehm and P. Vogel, "Physics of Massive Neutrinos", Cambridge University Press, Cambridge, England, 1992.
 - [18] P. Vogel, Phys. Rev. D **30**, 1505 (1984).
 - [19] B. Lie and F. Wilczek, Phys. Rev. D **25**, 766 (1982);
 - [20] P.B. Pal and L. Wolfenstein, Phys. Rev. D **25**, 766 (1982);
 - [21] R.E. Shrock, Nucl. Phys. B **206**, 359 (1982).
 - [22] C. Athanassopoulos et al., Nucl. Instr. Meth. A **388**, 149 (1997).
 - [23] L.B. Auerbach et al., Phys. Rev. C **66**, 015501 (2002).
 - [24] E. Kolbe, K. Langanke, F.-K. Thiehmman, and P. Vogel, Phys. Rev. C **52**, 3437 (1995).
 - [25] G. Garvey, E. Kolbe, K. Langanke, and S. Krewald , Phys. Rev. C **48**, 1919 (1993).
 - [26] C.J. Horowitz, H. Kim, D.P. Murdock, and S. Pollock, Phys. Rev. C **48**, 3078 (1993).
 - [27] B.I.S. van der Ventel and J. Piekarewicz, Phys. Rev. C **69**, 035501 (2004).
 - [28] M.C. Martinez et al., Phys. Rev. C **73**, 024607 (2006).
 - [29] T. Itoga et al., "Neutron Production from Thin Target of Carbon and Iron by 70 MeV Protons", <http://www.ndc.jaea.go.jp/nds/proceedings/2004>.
 - [30] A. Aguilar et al., Phys. Rev. D **64**, 112007 (2001).
 - [31] C. Athanassopoulos et al., Phys. Rev. C **58**, 2489 (1998).
 - [32] A.A. Aguilar-Arevalo et al., Nucl. Instr. Meth. Phys. Res. A **599**, 28 (2009).
 - [33] R.B. Patterson et al., Nucl. Instr. Meth. Phys. Res., A **608** (2009).
 - [34] A.A. Aguilar-Arevalo et al., arXiv:0806.1449.
 - [35] A.A. Aguilar-Arevalo et al., Phys. Rev. Lett. **103**, 111801 (2009); arXiv:0904.1958.
 - [36] C. Amsler et al., Review of Particle Physics, Phys. Lett. B **667**, 1 (2008).
 - [37] R.P. MacDonald et al., Phys. Rev. D **78**, 032010 (2008); A. Hillairet, Nucl. Phys. A **844**, 63C (2010).
 - [38] B. Kayser, Phys. Rev. D **26**, 1662 (1982).
 - [39] J.F. Nieves, Phys. Rev. D **26**, 3152 (1982).
 - [40] D. Gorbunov and M. Shaposhnikov, JHEP 0710, 015 (2007).
 - [41] A. Atre et al., JHEP **0905**, 030 (2009); arXiv:0901.3589.
 - [42] Y. Asano et al., Phys. Lett. B **104**, 84 (1981).
 - [43] C. Y. Pang et al., Phys. Rev. D **8**, 1989 (1973).
 - [44] R. Abela et al., Phys. Lett. B **105**, 263 (1981).
 - [45] R.S. Hayano et al., Phys. Rev. Lett. **49**, 1305 (1982).
 - [46] P. Kalyniak and J.N. Ng, Phys. Rev. D **25**, 1305 (1982).
 - [47] M.S. Dixit et al., Phys. Rev. D **27**, 2216 (1983).
 - [48] S.E. Derenzo, Phys. Rev. **181**, 1854 (1969).
 - [49] G. Bernardi et al., Phys. Lett. **166B**, 479 (1986).
 - [50] P. Abreu et al., Z. Phys. C **74**, 57 (1997).
 - [51] D. Buskulic et al., Phys. Rep. **216**, 253 (1992).
 - [52] V. Fanti et al., Nucl. Instrum. Meth. A **574**, 433 (2007).
 - [53] See for example, S.Adler et al., Phys. Rev. D **77**, 052003 (2008).
 - [54] J. Altegoer et al., Nucl. Instrum. Meth. A **404**, 96 (1998).
 - [55] C.T. Kullenberg et al., Phys. Lett. B **682**, 177 (2009).

- [56] S. Amerio et al., Nucl. Instrum. Meth. **A 523**, 275 (2004).
- [57] E. Calligarich et al., Jour. Phys.: Conf. Serie **203**, 012110 (2010).
- [58] See , for example, M. Soderberg, AIP Conf. Proc. **1189**, 83 (2009).
- [59] S.R. Mishra, R. Petti, and C. Rosenfeld, arXiv:0812.4527 [hep-ex].
- [60] I Stancu et al., arXiv:0910.2698 [hep-ex].
- [61] L.B. Auerbach et al., Phys. Rev. D **63**, 112001 (2001).
- [62] S.N. Gninenko and N.V. Krasnikov, Phys. Lett. **B 450**, 165 (1999).
- [63] J. Altegoer et al., Phys. Lett. **B 428**, 197 (1998); S.N. Gninenko and N.V. Krasnikov, Phys. Lett. **B 427**, 307 (1998).
- [64] A.D. Dolgov, Phys. Rept. **370**, 333 (2002).